



# The Sir4 H-BRCT domain interacts with phospho-proteins to sequester and repress yeast heterochromatin

Ishan Deshpande<sup>1,2,†,‡</sup>, Jeremy J Keusch<sup>1,‡</sup> , Kiran Challa<sup>1</sup>, Vytautas Iesmantavicius<sup>1</sup>, Susan M Gasser<sup>1,2</sup> & Heinz Gut<sup>1,\*</sup> 

## Abstract

In *Saccharomyces cerevisiae*, the silent information regulator (SIR) proteins Sir2/3/4 form a complex that suppresses transcription in subtelomeric regions and at the homothallic mating-type (HM) loci. Here, we identify a non-canonical BRCA1 C-terminal domain (H-BRCT) in Sir4, which is responsible for tethering telomeres to the nuclear periphery. We show that Sir4 H-BRCT and the closely related Dbf4 H-BRCT serve as selective phospho-epitope recognition domains that bind to a variety of phosphorylated target peptides. We present detailed structural information about the binding mode of established Sir4 interactors (Esc1, Ty5, Ubp10) and identify several novel interactors of Sir4 H-BRCT, including the E3 ubiquitin ligase Tom1. Based on these findings, we propose a phospho-peptide consensus motif for interaction with Sir4 H-BRCT and Dbf4 H-BRCT. Ablation of the Sir4 H-BRCT phospho-peptide interaction disrupts SIR-mediated repression and perinuclear localization. In conclusion, the Sir4 H-BRCT domain serves as a hub for recruitment of phosphorylated target proteins to heterochromatin to properly regulate silencing and nuclear order.

**Keywords** Dbf4; heterochromatin; SIR complex; Sir4 BRCT domain; Tom1

**Subject Categories** Chromatin, Transcription & Genomics; DNA Replication & Repair; Structural Biology

**DOI** 10.15252/embj.2019101744 | Received 8 February 2019 | Revised 24 July 2019 | Accepted 11 August 2019 | Published online 12 September 2019

**The EMBO Journal (2019) 38: e101744**

## Introduction

Chromatin-mediated silencing is critical for eukaryotic genome stability and cell survival. In budding yeast, *S. cerevisiae*, silent chromatin is maintained by the silent information regulator (SIR) complex which represses transcription in subtelomeric regions and the homothallic

mating-type loci (Rine & Herskowitz, 1987; Aparicio *et al*, 1991; Hecht *et al*, 1995; Kueng *et al*, 2013). The SIR complex, composed of the NAD<sup>+</sup>-dependent histone deacetylase Sir2, the histone binding protein Sir3, and the 152 kDa scaffold protein Sir4, serves as a model system to study epigenetically silenced heterochromatin in higher eukaryotes (reviewed in refs Gartenberg & Smith, 2016; Oppikofer *et al*, 2013). Repression of genes in *S. cerevisiae* is initiated by DNA-binding proteins repressor activator protein 1 (Rap1) (Shore *et al*, 1987; Moretti *et al*, 1994), ARS-binding factor 1 (Abf1) (Sussel & Shore, 1991), and origin recognition complex subunit 1 (Orc1) (Brand *et al*, 1987), which recognize specific DNA sequences located in silencer elements or telomeric repeats. Binding of these factors initiates chromatin repression by the recruitment of Sir1 and/or a heterotrimeric SIR complex that can spread along the chromatin fiber by oligomerization (Rudner *et al*, 2005; Cubizolles *et al*, 2006; Swygert *et al*, 2018). Central to nucleation is Rap1, which binds with high affinity to silencer elements and telomeric DNA (Buchman *et al*, 1988); it then interacts with Sir4 to recruit Sir2 to nucleosomes, allowing Sir2 to deacetylate the N-terminal histone H4 tail (Moretti *et al*, 1994; Hecht *et al*, 1995; Imai *et al*, 2000; Tanner *et al*, 2000). Hypoacetylated histone H4, in particular the deacetylated H4K16 residue, serves as a high-affinity site for the Sir3 bromo-adjacent homology (BAH) domain, helping assemble the SIR2,3,4 complex on nucleosomes (Connelly *et al*, 2006; Onishi *et al*, 2007; Oppikofer *et al*, 2011). From such nucleation sites, successive histone deacetylation by Sir2, followed by Sir3 binding, and Sir3 homo- and heterodimerization with the Sir2-4 subcomplex, allows spreading of a repressed chromatin structure along the DNA fiber (Strahl-Bolsinger *et al*, 1997; Rusche *et al*, 2002; Kueng *et al*, 2013).

Sir proteins have been studied extensively over the last 25 years, and crystal structures of individual domains have been determined to understand function and structural organization of transcriptional silencing (reviewed in ref. Oppikofer *et al*, 2013). Sir4 binds both Sir2 and Sir3, and therefore is thought to provide a scaffold for SIR complex formation (Hecht *et al*, 1996; Moazed *et al*, 1997; Rudner

<sup>1</sup> Friedrich Miescher Institute for Biomedical Research, Basel, Switzerland

<sup>2</sup> Faculty of Natural Sciences, University of Basel, Basel, Switzerland

\*Corresponding author. Tel: +41 61 696 70 38; Fax: +41 61 697 39 76; E-mail: heinz.gut@fmi.ch

<sup>‡</sup>These authors contributed equally to this work

<sup>†</sup>Present address: Department of Pharmaceutical Chemistry, University of California San Francisco, San Francisco, CA, USA

[The copyright line of this article was changed on 26 September 2019 after original online publication.]

et al, 2005). Sir4 comprises several well-studied domains (Figs 1A and EV1). The Ku-binding motif (KBM, residues 104–115; green box in Fig 1A) of Sir4 is involved in recruiting telomerase to telomeres through interaction between telomere-bound Sir4 and the Ku-telomerase complex (Schober et al, 2009; Chen et al, 2018). yKu80/yKu70 interacts with Sir4 regions 1–270 and 747–1,358 to recruit the SIR complex to telomeres and facilitates anchoring of silenced chromatin at the nuclear periphery (Tsukamoto et al, 1997; Laroche et al, 1998; Hediger et al, 2002; Luo et al, 2002; Roy et al, 2004; Schober et al, 2009). Sir4 is also required for Ku-mediated telomere lengthening and telomerase recruitment by interaction with the yKu70/80 heterodimer (Ferreira et al, 2011; Hass & Zappulla, 2015). The Sir2-interacting domain (SID, residues 737–893; blue box in Fig 1A) is important for SIR complex assembly and allosteric Sir2 deacetylase regulation (Hsu et al, 2013). The SID also provides a link to the nuclear periphery through interaction with the N-terminus of Mps3 (Bupp et al, 2007; Schober et al, 2009).

A more central Sir4 domain called partitioning and anchoring domain (PAD, residues 950–1,262; white box in Fig 1A) mediates binding of silenced heterochromatin to the nuclear envelope by binding a C-terminal fragment of Esc1 (establishes silent chromatin 1) (Ansari & Gartenberg, 1997; Andrulis et al, 2002; Taddei et al, 2004). The Sir4 PAD also interacts with the integrase of the Ty5 retrotransposon to integrate Ty5 into heterochromatic regions at telomeres and silent mating-type loci. Both, Esc1 and Ty5 seem to use a short proline-rich motif to bind the Sir4 PAD. Furthermore, Ty5 binding to Sir4 is mediated by post-translational modifications, such as phosphorylation (Zou et al, 1996; Dai et al, 2007; Brady et al, 2008). Finally, an N-terminal region of the Ubp10 deubiquitinase (residues 109–133) has been shown to interact with the Sir4 PAD to remove H2B ubiquitin marks, a prerequisite for heterochromatin formation (Reed et al, 2015; Zukowski et al, 2018).

Despite this rich array of interactors, little is known regarding the structural basis of Sir4 PAD function. In contrast, the C-terminal coiled-coil domain (CC, residues 1,271–1,347; magenta box in Fig 1A) of Sir4 is structurally well characterized. It drives Sir4 dimerization, which is thought to enable interactions with Sir3 and yKu70 (Chang et al, 2003; Murphy et al, 2003). The Rap1 interaction sites have been mapped to Sir4 regions 142–591 and 839–1,358, while Sir3 binding seems to require Sir4 residues 745–1,172 (Moretti et al, 1994; Luo et al, 2002). Interestingly, the C-terminal half of Sir4 is sufficient for repression at *HM* loci, whereas repression at telomeres requires the Sir4 N-terminus as well (Kueng et al, 2012). In conclusion, Sir4 can be described as a multi-domain protein that serves as the central scaffolding subunit of yeast heterochromatin.

BRCT domains (named after the BRCA1 C-terminal domain) are signaling modules that occur as single or tandem units in numerous proteins, especially those involved in DNA damage response (Leung & Glover, 2011). These 90–100 amino acid residue-long domains typically mediate protein–protein interactions. With the exception of the Dbf4 BRCT domain, all BRCT domains studied to date comprise a four-stranded parallel  $\beta$ -sheet surrounded by three  $\alpha$ -helices:  $\beta 1\alpha 1\beta 2\beta 3\alpha 2\beta 4\alpha 3$ . The Dbf4 BRCT domain, however, requires an additional N-terminal  $\alpha$ -helix that stabilizes the BRCT core and is therefore named helix-BRCT (H-BRCT) (Matthews et al, 2012). The Dbf4 H-BRCT occurs as a single unit and is thought to be deficient for phospho-peptide interaction.

Here, we identify a second example of the non-canonical H-BRCT domain in the Sir4 protein. We show that the Sir4 H-BRCT domain serves as the functional module of the Sir4 PAD, and we describe its interaction with phosphorylated targets. By X-ray crystallography, we establish the structural basis of Esc1-mediated recruitment of telomeres to the nuclear periphery by the Sir4 H-BRCT domain and describe how short phosphorylated sequence stretches in Ty5 and Ubp10 are recognized in a structurally similar fashion. Structure-guided point mutations in the Sir4 H-BRCT domain that disrupt its ability to bind cognate phospho-peptides phenotypically mimic *sir4* $\Delta$  and result in Sir4 mislocalization from perinuclear foci and an inability to silence transcription. Furthermore, we reveal a previously uncharacterized phospho-dependent interaction of the Sir4 H-BRCT domain with the Tom1 E3 ubiquitin ligase and the centromere-binding factor Cbf1. Based on these structural, biochemical, and cell biological findings, we hypothesize that the Sir4 H-BRCT domain provides a platform for proteins with a phosphorylated consensus motif [LIM]-x-[ST]-[SDE]-[PF]-[PLM], which in turn regulate heterochromatin silencing. We further demonstrate that the related Dbf4 H-BRCT also interacts selectively with phospho-peptides.

## Results

### Identification and structure determination of the Sir4 H-BRCT

In order to explore the mechanisms by which Sir4 carries out its various functions (Fig 1A), we performed a deep analysis of the Sir4 protein sequence by employing structural bioinformatics tools. We used HHPRED (Soding et al, 2005) to identify new putative domains in Sir4 by searching for remote homologs of known structure in the Protein Data Bank (PDB). To our surprise, there was a significant hit (probability 100%, *E*-value =  $1.9 \times 10^{-32}$ ) spanning Sir4 region ~960–1,080 (located in the first half of the PAD, orange box in Fig 1A) suggesting distant homology to the H-BRCT domain of the *S. cerevisiae* CDC7-DBF4 kinase regulatory subunit Dbf4 (sequence identity 18%). The Dbf4 H-BRCT domain has been shown to interact with the forkhead-associated domain 1 (FHA1) of the Rad53 kinase in a phosphorylation-independent manner (Matthews et al, 2012, 2014; PDB ID 3QBZ). Protein disorder prediction on the GeneSilico MetaDisorder server (Kozlowski & Bujnicki, 2012) confirmed the Sir4 sequence stretch ~950–1,100 to be structured. Multiple sequence alignments between several yeast Sir4 sequences and the H-BRCT domain of budding yeast Dbf4 were used (Fig 1B) for designing a Sir4 expression construct encompassing the putative domain. DNA coding for Sir4 residues 961–1,085 was cloned into an expression vector adding a N-terminal hexa-histidine tag, and the protein was expressed in *Escherichia coli* followed by purification to homogeneity. The protein crystallized in space group C2 with one molecule per asymmetric unit and the structure was determined by the single anomalous diffraction (SAD) method using a selenomethionine labeled derivative of the protein. The final structure was then obtained by refining the initial model against diffraction data collected from a native protein crystal at a resolution of 1.1 Å resulting in a model with good R-factors ( $R = 11.7\%$ ,  $R_{\text{free}} = 14.2\%$ ) and stereochemical parameters (Table EV1).

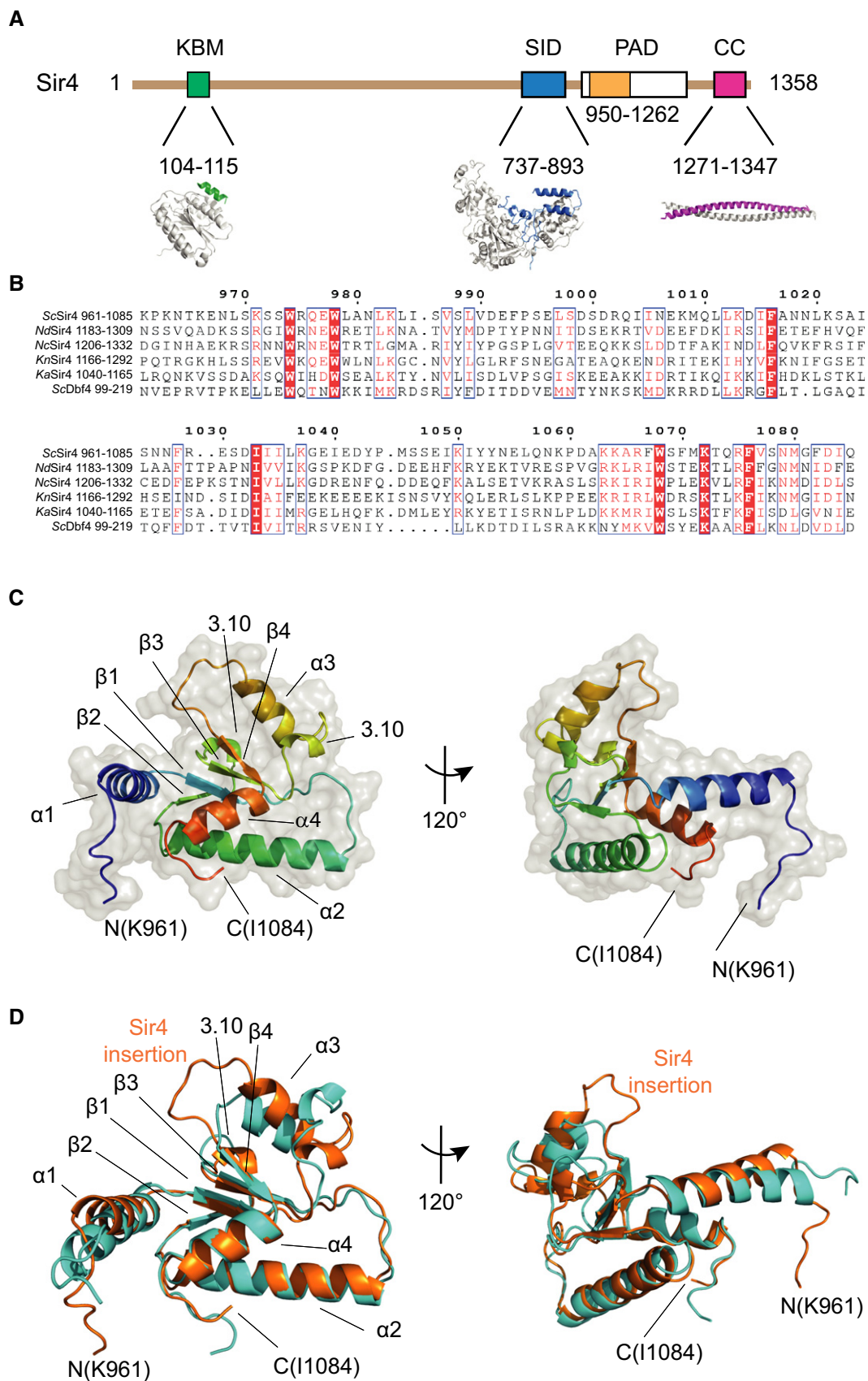


Figure 1.

**Figure 1. Crystal structure of Sir4 H-BRCT.**

- A Domain architecture of Sir4. Crystal structures have been determined for the Sir4 Ku80-binding motif (KBM) in complex with Ku80, the Sir4-interacting domain (SID) in complex with Sir2, and the Sir4 self-dimerization coiled-coil module (CC) (PDB 5Y59, 4IAO, and 1NYH, respectively). Sir4 H-BRCT (orange box, this work) locates to the first half of the partitioning and anchoring domain (PAD) which recruits silenced chromatin to the nuclear envelope.
- B ClustalO (Sievers *et al*, 2011) multiple sequence alignment of various yeast Sir4 proteins focusing on the putative new structural domain and comparison with *Saccharomyces cerevisiae* Dbf4 H-BRCT. Sir4 sequences: ScSir4 (*S. cerevisiae*, UniProt P11978), NdSir4 (*Naumovozyma dairenensis*, GOW8P4), NcSir4 (*Naumovozyma castellii*, GOVBN1), KnSir4 (*Kazachstania naganishii*, J7S2D5), and KaSir4 (*Kazachstania africana*, H2AVL7).
- C Scheme of the Sir4 H-BRCT crystal structure in two orientations rotated by  $\sim 120^\circ$  around a vertical axis. Colors gradually vary from blue (N-terminus) to red (C-terminus), while the surface is shown in gray (transparent). Termini and secondary structural elements are labeled.
- D Superposition of Sir4 H-BRCT (orange) onto the H-BRCT domain of Dbf4 (PDB 3QBZ, cyan) in two orientations as in (C). Secondary structural elements, termini, and the elongated Sir4 loop connecting helix  $\alpha 3$  and strand  $\beta 4$  are labeled.

**Overall structure of Sir4<sup>(961–1,085)</sup>**

The structure of Sir4<sup>(961–1,085)</sup> displays clear electron density at high resolution and folds into a BRCT-like fold with a four-stranded parallel  $\beta$ -sheet in the center surrounded by four  $\alpha$ -helices and two short stretches of 3.10-helices (Fig 1C). The structure superimposes well onto the structure of the H-BRCT domain of Dbf4 (PDB 3QBZ) with a r.m.s.d. of only 1.4 Å over 433 atoms (Fig 1D). Similar to the H-BRCT domain of Dbf4, Sir4<sup>(961–1,085)</sup> also possesses an additional  $\alpha 1$  helix at the N-terminus and has an elongated  $\alpha 2$  helix, thereby featuring the two unique structural elements which are different from canonical BRCT domain structures. Hence, we will refer to the newly discovered Sir4 domain from here onwards as H-BRCT. Besides the overall structural similarity of protein backbones, H-BRCT domains of Sir4 and Dbf4 differ in the conformation of loops between  $\beta$ -strands  $\beta 2$  and  $\beta 3$ , between strand  $\beta 3$  and helix  $\alpha 3$ , in the length of the loop between helix  $\alpha 3$  and strand  $\beta 4$  where a seven-residue insertion is found in Sir4, and in the position and angles of helices  $\alpha 1$  and  $\alpha 3$  (Fig 1D).

**Sir4 H-BRCT domain does not interact with Rad53 FHA1**

H-BRCT domains of Sir4 and Dbf4 are structurally very similar but Dbf4 residues critical for interaction with the FHA1 domain of Rad53 (black and blue asterisks in Fig 2A) are only partially conserved in Sir4. Nevertheless, we wondered whether Sir4 H-BRCT would also regulate Rad53 activity by binding to the FHA1 domain in a similar way. Recently, the crystal structure of Dbf4 H-BRCT in complex with the FHA1 domain of Rad53 bound to a CDC7 peptide was determined using an engineered single chain chimera of the two proteins revealing a bipartite interaction surface (Almawi *et al*, 2016). Superposition of Sir4 H-BRCT onto the Dbf4 H-BRCT-Rad53-CDC7 complex (Fig 2B) identified Dbf4 H-BRCT helix  $\alpha 1$  residues contributing to interface I (black dashed circle in Fig 2B) as partially conserved in Sir4, while interface II (blue dashed circle in Fig 2B), mainly formed by the loop connecting Dbf4 H-BRCT helix  $\alpha 3$  and strand  $\beta 4$ , was not conserved as a seven-residue insert replaces it (orange bar in Fig 2A). This comparatively longer Sir4 H-BRCT loop is quite flexible in the C2 crystal structure (Fig 2B) which accounts for the partial disorder of residues Asp1061 and Ala1062. The Sir4 H-BRCT loop lacks an aromatic residue corresponding to Tyr198 (Dbf4 H-BRCT, blue arrow in Fig 2A) which contributes most of the binding energy for the FHA1 domain (computed using PISA, <https://www.ebi.ac.uk/pdbe/pisa/>) in this region. The lysine residue of Sir4 H-BRCT at this position (Lys1064, orange arrow in

Fig 2A) cannot provide the hydrophobic surface necessary for binding and would prevent, along with the increased steric requirements of the longer Sir4 H-BRCT loop, any potential Rad53 FHA1 interaction. To test whether Sir4 H-BRCT interacts with Rad53 FHA1, we performed *in vitro* pull-down experiments. His-tagged Rad53 FHA1 immobilized on Ni-NTA magnetic beads failed to interact with untagged Sir4 H-BRCT, but interacted with Dbf4 H-BRCT (Fig EV2A). In addition, Sir4 H-BRCT and Rad53 FHA1 did not co-elute as a heterodimer as analyzed by size exclusion chromatography coupled with multi-angle light scattering (SEC-MALS; Fig EV2B and C). Therefore, we conclude that the H-BRCT domains of Sir4 and Dbf4 may bind different interactors.

**Structural basis of Sir4 H-BRCT interaction with Esc1, Ty5, and Ubp10 phospho-peptides**

Analysis of the electrostatic surface potential of Sir4 H-BRCT displayed a clearly defined basic patch formed by conserved residues Arg1066, Lys1072, and Arg1075, which was located in a pocket shaped by conserved helix  $\alpha 1$  residues Trp974 and Trp978, the elongated Sir4 H-BRCT loop 1,058–1,065 and the core of the H-BRCT domain (Fig 3A). Given that the Sir4 H-BRCT is found on the PAD, which has been shown to interact with several other proteins (Figs 1A and EV1), we hypothesized that the Sir4 H-BRCT domain is responsible for PAD interactions. Interestingly, the Ty5 motif that interacts with the first part of the Sir4 PAD has been shown to be dependent on a single phosphorylation site and a related proline-rich sequence identified in Esc1 also lost binding to Sir4 upon mutation of a serine to alanine (Dai *et al*, 2007; Brady *et al*, 2008). Based on these findings, we hypothesized that Sir4 H-BRCT recognizes a phospho-epitope on Esc1. To test this hypothesis, we used two phosphorylated Esc1 peptides for co-crystallization experiments with Sir4 H-BRCT encompassing a conserved proline-rich motif (IPSTDLPpSDPPSDKKEE and IPSTDLPSPDPPpSDKKEE, residues 1,443–1,458) which is part of the minimal sequence stretch (residues 1,440–1,473) mapped for interaction with Sir4 (Andrulis *et al*, 2002). These Esc1 phosphorylation sites (pS1450 and pS1454) were experimentally determined in a global analysis of cyclin-dependent kinase 1 substrates involved in cell cycle control in yeast (Holt *et al*, 2009). In addition, we performed co-crystallization experiments with Sir4 H-BRCT using the well-characterized Ty5 motif needed for Ty5 retrotransposon integration at heterochromatic loci in its Ser1095 phosphorylated state (pS1095, ESPPSLDSPSPNTSFNA, residues 1,087–1,103; Dai *et al*, 2007; Brady *et al*, 2008), and a proline-rich peptide that we identified in the Ubp10 sequence stretch

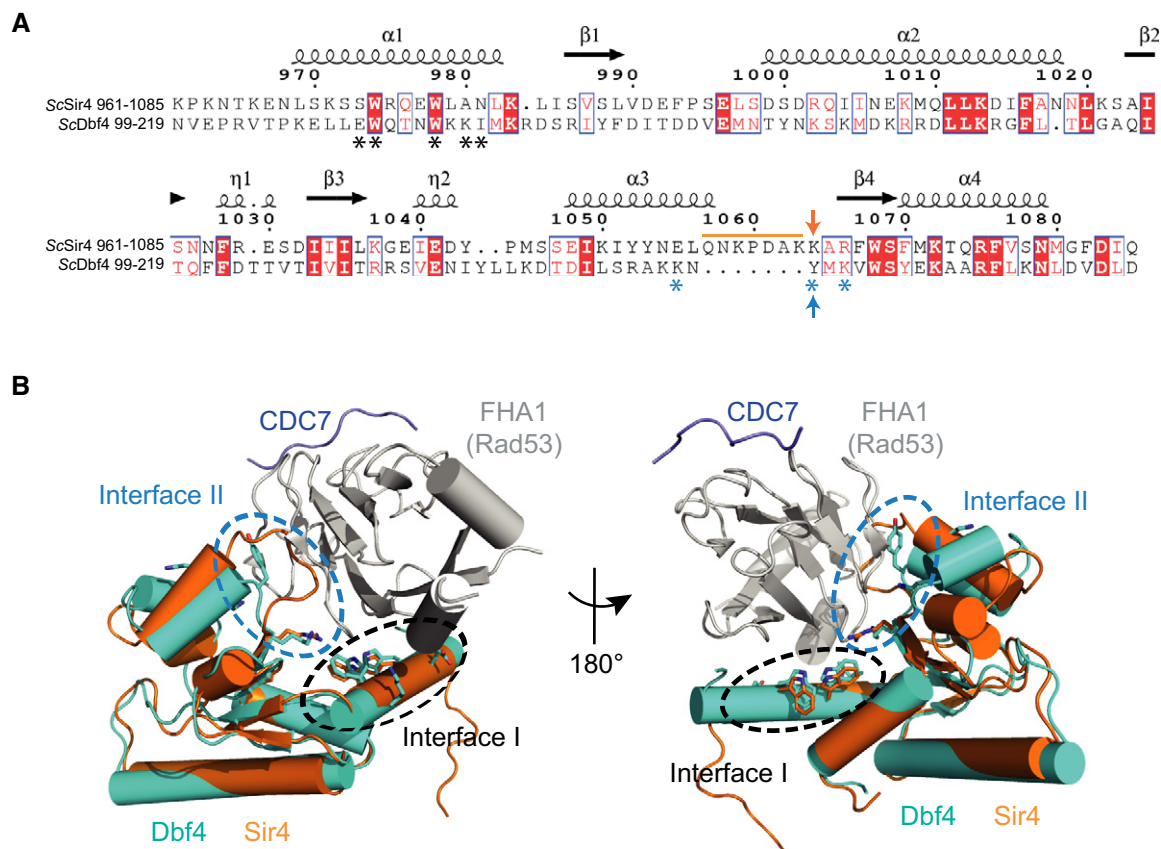


**Figure 2. Sir4 H-BRCT structural comparison with Dbf4 H-BRCT and Rad53 FHA1 binding.**

**A** Structure-based sequence alignment between H-BRCT domains of Sir4 (top) and Dbf4 (PDB 3QBZ, bottom). Secondary structural elements present in the Sir4 H-BRCT crystal structure are displayed above the Sir4 sequence ( $\alpha$ ,  $\alpha$ -helix;  $\beta$ ,  $\beta$ -strand;  $\eta$ , 3.10 helix). Dbf4 residues strongly contributing to Rad53 FHA1 binding are highlighted with black (interface I) and blue (interface II) asterisks. The elongated loop connecting helix  $\alpha$ 3 and strand  $\beta$ 4 in Sir4 H-BRCT is labeled with an orange bar, and the Tyr198 (Dbf4) to Lys1064 (Sir4) exchange is highlighted with colored arrows.

**B** Superposition of Sir4 H-BRCT (orange) onto the Dbf4-Rad53-CDC7 complex (cyan, gray, blue) (PDB 5T2S) in two orientations rotated by  $\sim 180^\circ$  around a vertical axis. Helices are displayed as barrels, and protein-protein interfaces between Dbf4 and FHA1 of Rad53 are highlighted with dashed circles in black (interface I) and blue (interface II).

(residues 109–133) that had been recently shown to interact with Sir4 (Zukowski *et al.*, 2018). Based on sequence comparisons with Esc1 and Ty5, we hypothesized that the Ubp10-Sir4 interaction might also be phosphorylation dependent and therefore used the Ubp10 peptide (LSTELSpTEPPSS, residues 117–128) in its Thr123 phosphorylated state (pT123).

Crystals were obtained, and structures of Sir4 H-BRCT in complex with Esc1<sup>pS1450</sup>, Ty5<sup>pS1095</sup>, and Ubp10<sup>pT123</sup> peptides were determined by the molecular replacement method at 2.5, 3.0, and 2.18 Å resolution, respectively (Table EV1). All three peptides interact with Sir4 H-BRCT using the positively charged patch created by Arg1066, Lys1072, and Arg1075 which is surrounded by helix  $\alpha$ 1/ $\alpha$ 4 and  $\beta$ -strand  $\beta$ 4, and feature a highly similar conformation (Figs 3B and EV3). We did not obtain crystals of Sir4 H-BRCT in complex with Esc1<sup>pS1454</sup> peptide and therefore only focused on the Esc1<sup>pS1450</sup> peptide in subsequent experiments. The Esc1 pSer1450 phospho-group is tightly anchored through electrostatic interactions with Arg1066, Trp1068, and Lys1072 side chains. It allows the peptide to form a sharp turn to use the aromatic indole rings of Sir4 H-BRCT

Trp974 and Trp978 for hydrophobic interaction with Esc1 residues Leu1448 and Pro1452/1453. This way, the Pro1449 carbonyl group is in ideal hydrogen bonding distance (2.9 Å) to NE1 atoms of the same Trp974/978 residues, while the Leu1448 carbonyl can interact with the Arg1066 guanidinium group (Fig 3C). In the case of Ty5, the pS1095 phospho-group is shifted by one residue toward the double proline motif and is therefore bound by Sir4 H-BRCT residues Lys1072 and Arg1075, while the Ser1094 hydroxyl group directly contacts Arg1066 (which is also in contact with a sulfate ion from the crystallization buffer; Fig 3D and EV3B). Other contacts are similar as in the case of Esc1, with Ty5 Leu1092 and Pro1096/1097 making hydrophobic contacts with Sir4 H-BRCT Trp974/978, and Ty5 Asp1093 hydrogen bonding the same residues using its carbonyl group. The Ubp10<sup>pT123</sup> peptide binds in a similar way by positioning the phospho-group (this time located on a threonine) in the same place as the Esc1 peptide, where it interacts with Arg1066, Trp1068, and Lys1072 (Fig 3E). The overall binding mode is again conserved with Ubp10, where Leu121 and Pro125/126 make hydrophobic contacts with Sir4 H-BRCT Trp974/978 and Ubp10

Ser122 mediates hydrogen bonding to the same residues using its carbonyl group. In addition, the Ubp10 Glu124 side chain is long enough to hydrogen bond to Sir4 Arg1075, while the Ser118 backbone carbonyl makes an additional weak hydrogen bond to the Arg1066 side chain of Sir4 H-BRCT, extending the Sir4-binding sequence motif toward the N-terminus of the peptide.

Having characterized the binding mode of Sir4 H-BRCT to Esc1, Ty5, and Ubp10 phospho-peptides at atomic resolution, we used microscale thermophoresis (MST) to determine the affinity of Sir4 H-BRCT for these peptides in phosphorylated and non-phosphorylated states (Fig 3F, and Tables EV2 and EV3). All three peptides bound Sir4 H-BRCT domain in a phosphorylation-dependent

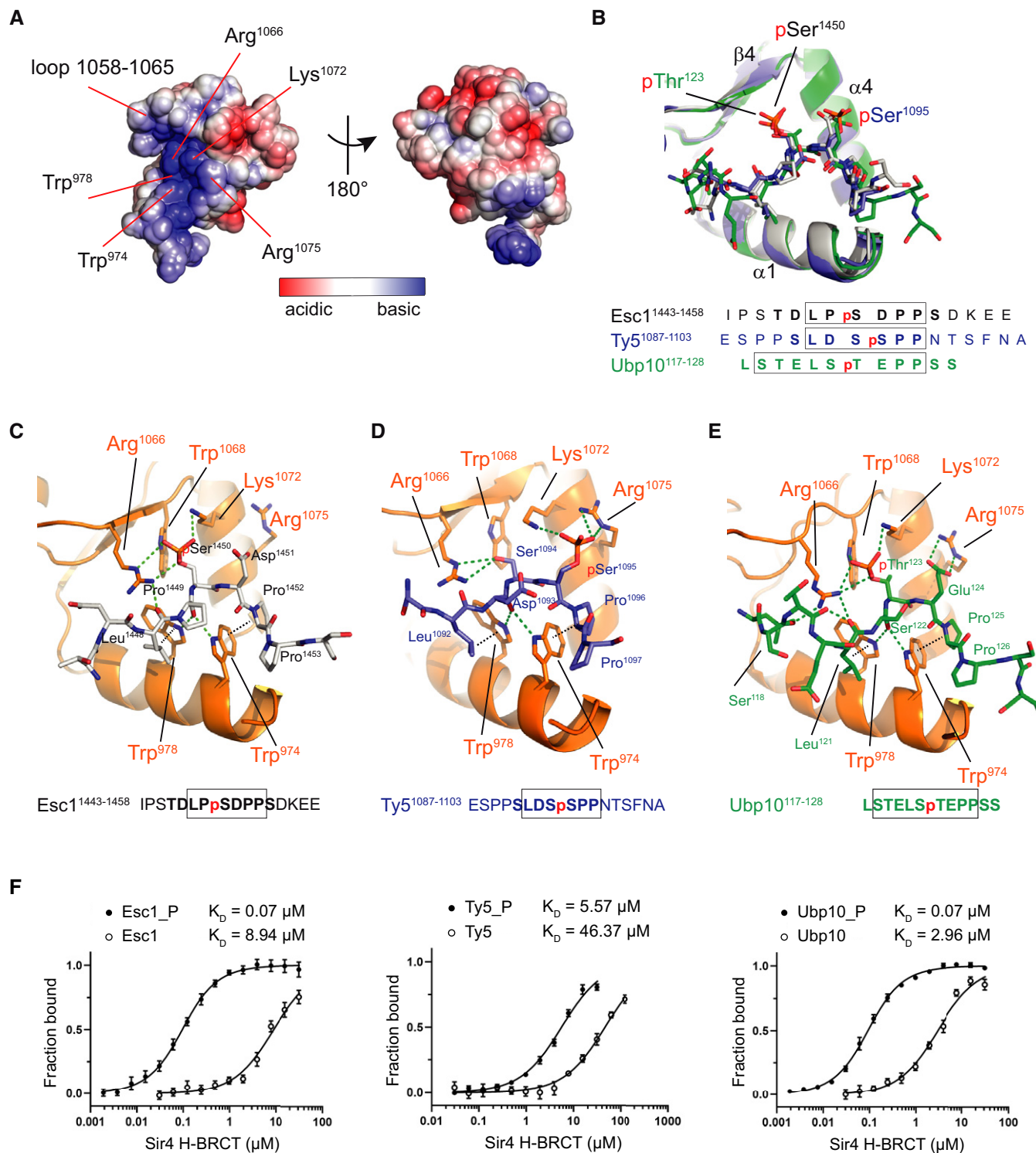


Figure 3.

**Figure 3. Structural basis of Sir4 H-BRCT interaction with phospho-peptides.**

- A The electrostatic surface potential covering a range from  $-4$  kT/e (red/acidic) to  $+4$  kT/e (blue/basic) is mapped onto the Sir4 H-BRCT structure to highlight the basic patch on the H-BRCT surface. Sir4 H-BRCT is shown in two orientations rotated by  $180^\circ$ , and selected residues are labeled.
- B Superpositions of Sir4 H-BRCT-Esc1<sup>pS1450</sup> (gray cartoon, peptide as sticks in atom colors), Sir4 H-BRCT-Ty5<sup>pS1095</sup> (blue cartoon, peptide as sticks in atom colors), and Sir4 H-BRCT-Ubp10<sup>pT123</sup> (green cartoon, peptide as sticks in atom colors) peptide complex structures reveal the highly similar conformation of peptide binders. Esc1<sup>pS1450</sup>, Ty5<sup>pS1095</sup>, and Ubp10<sup>pT123</sup> peptides used for co-crystallization are indicated with residues modeled in the structures in bold and residues that contribute most binding to Sir4 H-BRCT boxed.
- C Detailed view of the Sir4 H-BRCT-Esc1<sup>pS1450</sup> peptide interaction. Sir4 H-BRCT is displayed as orange model with residues involved in peptide binding shown as sticks (orange, atom colors). The Esc1<sup>pS1450</sup> peptide is presented as sticks in gray (atom colors). Electrostatic interactions are highlighted with green dotted lines, while main hydrophobic contacts are shown as dotted lines in black.
- D Detailed view of the Sir4 H-BRCT-Ty5<sup>pS1095</sup> peptide interaction. Sir4 H-BRCT is displayed as in (C), while the Ty5<sup>pS1095</sup> peptide is presented as sticks in blue (atom colors). Protein-peptide interactions are labeled as in (C).
- E Detailed view of the Sir4 H-BRCT-Ubp10<sup>pT123</sup> peptide interaction. Sir4 H-BRCT is displayed as in (C), while the Ubp10<sup>pT123</sup> peptide is presented as sticks in green (atom colors). Protein-peptide interactions are labeled as in (C).
- F MST analysis of the binding interactions between Sir4 H-BRCT and Cy5-labeled phospho (filled circles) and non-phospho-peptides (empty circles) from Esc1, Ty5, and Ubp10.  $K_D$  = equilibrium dissociation constant.  $\Delta F_{\text{norm}}$  values were divided by the amplitude of the saturation level, resulting in the fraction bound (from 0 to 1) for each data point. Data are represented as the mean  $\pm$  SEM from  $\geq 3$  independent measurements.

manner with an equilibrium dissociation constant,  $K_D$ , in the nanomolar range for Esc1 and Ubp10 ( $0.07 \mu\text{M}$ ) and low micromolar range for Ty5 ( $5.57 \mu\text{M}$ ).

#### Sir4 RKR residues are critical for Sir4 localization and telomere clustering at the nuclear periphery

In budding yeast, heterochromatin is anchored to the nuclear periphery through the inner membrane-associated proteins Esc1 (Andrulis *et al*, 2002; Hediger *et al*, 2002; Taddei *et al*, 2004) and Mps3 (Bupp *et al*, 2007; Schober *et al*, 2009). Cells lacking Esc1 fail to tether heterochromatin to the nuclear envelope and are characterized by dispersed telomeres and telomere-associated SIR foci (Hediger *et al*, 2002; Gartenberg *et al*, 2004; Taddei *et al*, 2004). Our structural and biochemical insights highlighted the importance of the Sir4 H-BRCT positively charged triad (Arg1066, Lys1072 and Arg1075) in binding Esc1, Ty5, and Ubp10 phospho-peptides. To test the functional significance of phospho-peptide binding, we mutated these three residues to alanines in Sir4 (hereafter named *sir4* RKR), thereby disrupting the phospho-peptide interaction, and tested telomere recruitment in the *sir4* RKR mutant. We tagged Nup49, an integral nuclear pore protein as a marker of the nuclear envelope (NE), with red fluorescent protein (RFP), and either Sir4 wild-type (wt) or the *sir4* RKR mutant with green fluorescent protein (GFP) and expressed fusion proteins under their endogenous promoters. Yeast strains used are summarized in Table EV4. We then analyzed localization of Sir4-GFP and Nup49-RFP in both wt and RKR strains by fluorescence microscopy (Fig 4A–C). As expected in wt cells, Sir4 clustered in 4–6 foci per nucleus representing the Esc1-mediated telomere assembly at the NE. However, Sir4 protein levels were reduced in the RKR mutant as seen by a reduced number of Sir4 foci (1–3) per nucleus and a  $\sim 30\%$  decrease in the total nuclear intensity of the Sir4-GFP signal (Fig 4B, dark gray circles). Since Sir4 protein levels greatly impact Sir4 function (Cockell *et al*, 1995; Smith *et al*, 1998), we performed competition experiments to study the role of Sir4 RKR mutations without affecting Sir4 protein levels. In our competition assay, we overexpressed the Sir4 H-BRCT domain in wild-type yeast, to allow the overexpressed Sir4 H-BRCT fragment to compete with endogenous Sir4 for binding to Sir4's phosphorylated interactors. Importantly, overexpression of the Sir4 H-BRCT domain did not reduce

endogenous Sir4 protein levels (Fig 4B, orange circles), but caused a  $\sim 40\%$  reduction in Sir4-containing telomere clusters at the NE (Fig 4C, orange bar). Overexpression of the mutant Sir4 RKR H-BRCT showed no Sir4 focus mislocalization (Fig 4C, light blue bar). Notably, protein levels of overexpressed Sir4 wt and mutant H-BRCT domains were similar and both domains showed similar biochemical characteristics when purified to homogeneity (Fig EV4). Given that Sir4 coincides with telomeric foci, our observations argue that mutations that ablate the binding of Sir4 H-BRCT to phospho-proteins alter both Sir4 localization and telomere recruitment to the nuclear rim.

#### Sir4 H-BRCT RKR residues are critical for heterochromatin silencing

To test the role of the RKR motif in heterochromatin silencing, we performed Sir4 H-BRCT competition experiments using previously established silencing assays (Marshall *et al*, 1987; Kueng *et al*, 2012). Yeast strains used in this study are summarized in Table EV4. To monitor silencing at telomeres, we scored the expression of a *URA3* reporter gene inserted at telomere 7L using a colony growth assay on media lacking uracil (Fig 4D). We used a strain that lacks Ppr1, a transcription factor that induces high-level *URA3* expression in the absence of uracil (Renauld *et al*, 1993). As expected, in cells transformed with an empty plasmid, endogenous Sir4 was able to silence the *URA3* reporter gene resulting in lack of growth on uracil-deficient media (Fig 4D, row 1). Overexpression of wt Sir4 H-BRCT was able to disrupt repression of the reporter gene to allow colony growth (Fig 4D, row 2), phenocopying a strain lacking *sir4* (Fig 4D, row 4). On the other hand, overexpression of the mutant Sir4 RKR H-BRCT showed no *URA3* silencing defect (Fig 4D, row 3). Therefore, competing out phospho-interactors of the Sir4 H-BRCT domain disrupted SIR-mediated silencing in subtelomeric domains.

We next tested whether the Sir4 RKR motif is essential for silencing a reporter gene in another chromosomal context. For this purpose, we used a *HMR-EΔB::TRP1* reporter strain that lacks the B sequence (Abf1-binding site) within the E silencer (Brand *et al*, 1987) at the endogenous *HMR* locus (Fig 4E). Similar to the subtelomeric silencing defect, overexpression of wt Sir4 H-BRCT, but not Sir4 RKR H-BRCT, disrupted repression of the *TRP1* reporter

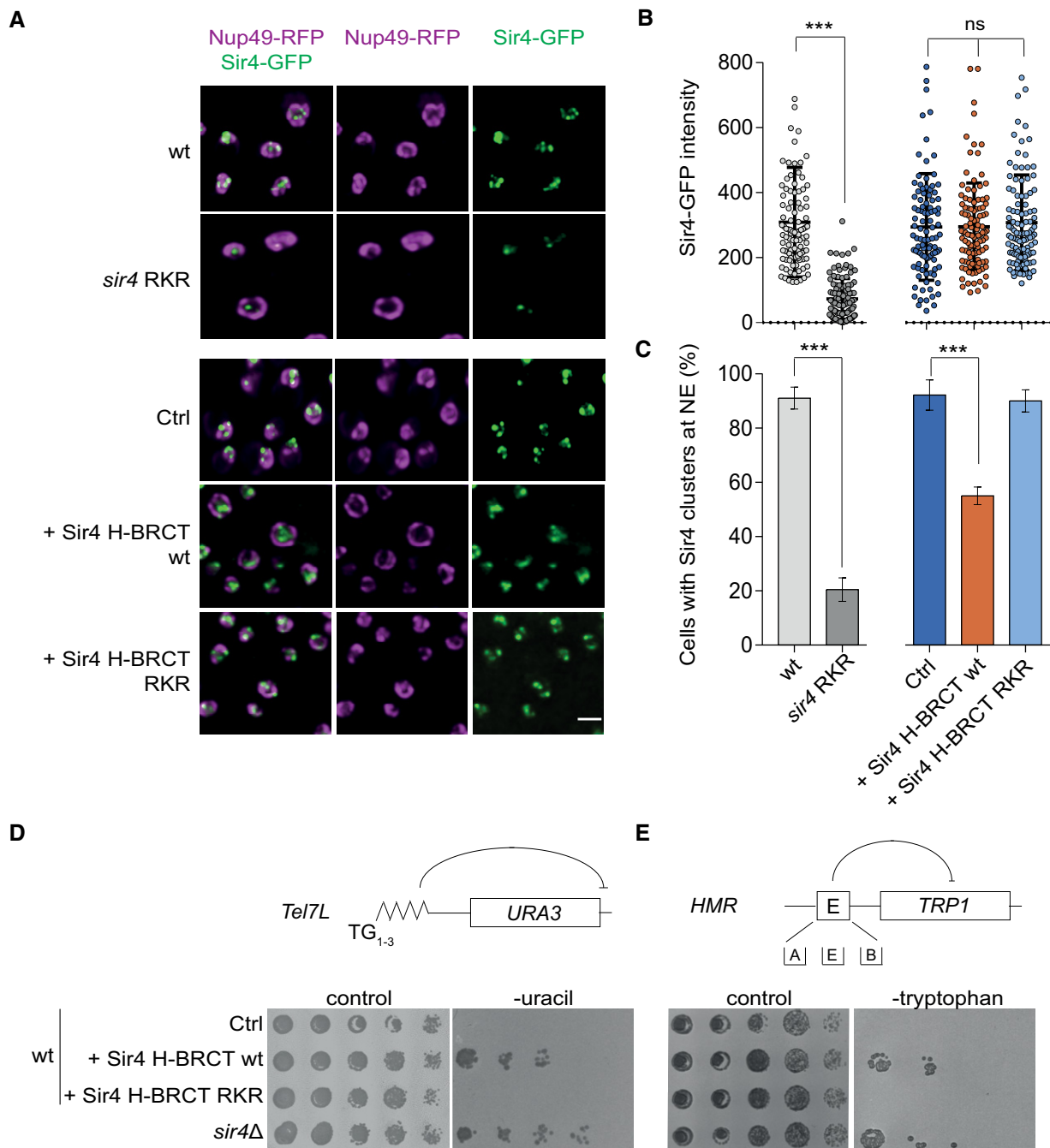


**Figure 4. Sir4 RKR residues are important for heterochromatin silencing and proper localization of Sir4 at the nuclear periphery.**

A Example images of Nup49-RFP Sir4-GFP in wild-type (wt) cells (GA-10372; row 1); *sir4* RKR cells (GA-10373; row 2); wt cells transformed with either empty plasmid (row 3), plasmid overexpressing wt Sir4 H-BRCT (row 4), or plasmid overexpressing RKR mutant Sir4 H-BRCT (row 5). The bar indicates 2  $\mu$ m.

B Quantification of mean fluorescence intensity of Sir4-GFP using > 100 cells. Error bars show the SD from three independent experiments.

C Quantification of cells containing Sir4 clusters at the nuclear envelope (NE). Data are represented as mean  $\pm$  SD from three independent experiments where > 100 cells were counted.

D Top: Schematic representation of the TEL7L::URA3 reporter used to assay silencing at telomeres. Bottom: wt cells (GA-503) transformed with either an empty plasmid (row 1), plasmid overexpressing wt Sir4 H-BRCT (row 2), or plasmid overexpressing RKR mutant Sir4 H-BRCT (row 3). Cells lacking endogenous *sir4* (GA-5822) (row 4). Cells were grown in the absence of uracil and plated as 1:5 serial dilutions onto control YPAD or YPAD lacking uracil plates and imaged after 2 days.

E Top: Schematic representation of the HMR-E $\Delta$ B::TRP1 reporter gene locus used for assaying silencing at the HMR locus. Bottom: wt cells (GA-485) transformed with plasmids as in panel D. Cells lacking endogenous *sir4* (GA-6888) (row 4). Cells were grown in the absence of tryptophan and plated as 1:5 serial dilutions onto YPAD or YPAD lacking tryptophan plates and imaged after 2 days.

Data information: (B, C) \*\*\**P* < 0.001 (*t*-test).



gene at *HMR* and phenocopied a complete loss of *sir4*. In conclusion, these silencing assays suggest that the Sir4 RKR motif, which is essential for phospho-peptide interaction, is required both for heterochromatin silencing at telomeric and *HMR* loci, and for Sir4 focus formation at the NE.

### Establishing the nuclear phospho-proteome of Sir4 interactors by mass spectrometry

Based on the versatility of the Sir4 H-BRCT domain in binding three different phospho-peptides (Esc1, Ty5, and Ubp10), we hypothesized that the H-BRCT domain might act as a general platform to recruit a variety of phosphorylated proteins to heterochromatin. To examine putative novel phospho-dependent interactors of the Sir4 H-BRCT domain globally, we performed immunoprecipitation followed by mass spectrometric analysis (IP-MS). The C-terminally Myc-tagged Sir4 H-BRCT domain, either wt or harboring phospho-peptide binding-deficient R1066A, K1072A, R1075A mutations, was expressed in *trans* from a plasmid in a *sir4Δ* background strain to specifically enrich for RKR-dependent interactors of the H-BRCT domain. Interacting proteins were immunoprecipitated from yeast cell extracts using ChromoTek Myc-Trap\_MA beads in the presence of phosphatase inhibitors, and the purified material was reduced, alkylated, and digested for subsequent analysis by liquid chromatography-tandem mass spectrometry (LC-MS/MS; Fig 5A). Results are visualized in a volcano plot highlighting nuclear proteins enriched in Sir4 wt but not in Sir4 RKR mutant cells implying specific, phosphorylation-dependent interaction of identified proteins with the Sir4 H-BRCT domain (upper right quadrant; Fig 5B).

As expected, we found a strong enrichment of Esc1 in the wt, but not the mutant, Sir4 H-BRCT interactome. This validates our experimental approach and argues that Esc1 binds the Sir4 H-BRCT domain in a phosphorylation- and RKR motif-dependent manner. In addition, a set of RNA processing proteins previously not known to interact with Sir4 was identified. The U6 snRNA-associated Sm-like protein LSM6 and the DNA-directed RNA polymerase II subunit RPB1 (RPO21) were moderately enriched (1.68- and 1.66-fold compared to Esc1), while the mRNA-capping enzyme subunit beta protein CET1 and the ribosome biogenesis protein TSR1 were enriched just above threshold level. Interestingly, the E3 ubiquitin ligase Tom1 and the centromere-binding factor Cbf1 were highly enriched (3.61- and 3.78-fold, respectively, compared to Esc1) and are therefore likely to be novel Sir4 interactors.

To identify candidate phospho-peptides in Tom1 and Cbf1 that may be involved in Sir4 H-BRCT binding, we compared the observed phosphorylation sequences from our mass spectrometry analyses with consensus interaction motifs in Esc1, Ty5, and Ubp10. These putative interaction sites in Tom1 and Cbf1 were then tested for Sir4 H-BRCT binding using MST. Cy5 labeled Tom1 peptide 2,370–2,381 (HSREIDpSFLEA) and Cbf1 peptide 149–160 (SLEGMTpSSPMES) bound Sir4 H-BRCT with affinities of  $K_D = 35.06 \mu\text{M}$ , and  $15.96 \mu\text{M}$ , respectively. Since the measured affinities between Sir4 H-BRCT and Tom1/Cbf1 phospho-peptides were relatively weak, it is possible that there is an additional interface between Sir4 and Tom1/Cbf1 proteins. Nevertheless, the Sir4 binding was dependent on the presence of the phospho-group on Tom1 and Cbf1 peptides (Fig 5C, and Tables EV2 and EV3).

Because ubiquitination dynamics and protein turnover have been implicated in telomeric silencing (Burgess *et al.*, 2012), we examined further if endogenous Sir4 stably binds Tom1 by performing co-immunoprecipitations. For this, we constructed HA-tagged Tom1 and Myc-tagged Sir4 in either wt or RKR backgrounds. Interacting factors were immunoprecipitated from whole cell extracts using Myc-Trap magnetic beads (ChromoTek), and the co-precipitation of Tom1-HA was monitored with an anti-HA antibody (Fig 5D). Indeed, Tom1-HA co-immunoprecipitated with wt Sir4-Myc (lane 1) but failed to co-immunoprecipitate with the mutant Sir4-RKR-Myc (lane 2). To confirm our hypothesis that the Tom1-Sir4 interaction is phosphorylation dependent, we treated our IP samples with lambda phosphatase to remove phosphorylation. In agreement with our IP-MS and MST results, the Sir4-Tom1 interaction was lost when cell extracts were treated with phosphatase, providing strong evidence that the Sir4-Tom1 interaction is phosphorylation-dependent. In conclusion, we identify Tom1 as a novel interactor of the Sir4 PAD domain and provide evidence that this interaction occurs through the Sir4 H-BRCT domain in a phosphorylation-dependent manner.

### Dbf4 H-BRCT is also a phospho-peptide-binding module

With the exception of the elongated Sir4 H-BRCT loop encompassing residues 1,058–1,065, which includes the tyrosine (Dbf4, Tyr198) to lysine (Sir4, Lys1064) switch (Fig 2), there is high overall structural conservation between the Dbf4 H-BRCT and Sir4 H-BRCT domains. We therefore explored whether Dbf4 H-BRCT might also bind a range of phosphorylated target peptides like those that interact with Sir4 H-BRCT. The superposition of Dbf4 H-BRCT and Sir4 H-BRCT domains reveals that only Arg1066, the key phospho-anchoring residue in the Sir4 phospho-epitope-binding region involved in Esc1, Ubp10, Tom1, and Cbf1 interaction, is replaced by a lysine residue in Dbf4 H-BRCT (Lys200, black arrow in Fig 6A). This conservative change from an arginine to a lysine keeps the positive charge for electrostatic interaction with a phospho-group, which is a prerequisite to induce the sharp turn that brings the hydrophobic residues flanking the phospho-site in close contact with the double tryptophan motif (Trp974/978 in Sir4, Trp112/116 in Dbf4) located on the N-terminal  $\alpha$ -helix of H-BRCTs. We tested whether Esc1<sup>pS1450</sup>, Ty5<sup>pS1095</sup>, Ubp10<sup>pT123</sup>, Tom1<sup>pS2376</sup>, and Cbf1<sup>pS155</sup> peptides bind to purified Dbf4 H-BRCT using MST (Figs 6B and EV5, and Tables EV2 and EV3). We calculated equilibrium dissociation constants,  $K_D$ , of 0.9, 0.63, 75.46, and 172.43  $\mu\text{M}$  for Esc1<sup>pS1450</sup>, Ubp10<sup>pT123</sup>, Tom1<sup>pS1095</sup>, and Cbf1<sup>pS155</sup> peptides, respectively, indicating a broad range from tight to weak binding. Binding was completely dependent on the phospho-group, given that non-modified peptides failed to interact. On the other hand, the Ty5 pS1095 peptide, in which the phospho-group is shifted toward the C-terminus by one residue, had no detectable affinity. Intriguingly, in our Sir4 H-BRCT-Ty5<sup>pS1095</sup> co-crystal structure, we resolved a sulfate ion, which may serve as a Ty5 S1094 phosphorylation mimic, interacting with Sir4 R1066. Therefore, we mimicked MST binding assays in the presence of sulfate ions to mimic phosphorylation on S1094, to test whether pS1094/pS1095 is a more appropriate motif for Dbf4 H-BRCT binding to the Ty5 peptide. Indeed, we were able to measure weak binding ( $K_D = 66 \mu\text{M}$ ) between Dbf4 H-BRCT and Ty5<sup>pS1095</sup> peptide in the presence of sulfate ions (Fig EV6). Binding remained dependent

on the phosphorylation of S1095 since the peptide lacking phospho-modification showed no measurable binding, but these results suggest a preference for a double phosphorylation motif in Dbf4

H-BRCT interactions. Importantly, in comparison with Sir4 H-BRCT, we note that all ligands except Tom1 have roughly a tenfold lower  $K_D$  for their interaction with the Dbf4 H-BRCT domain. We assume

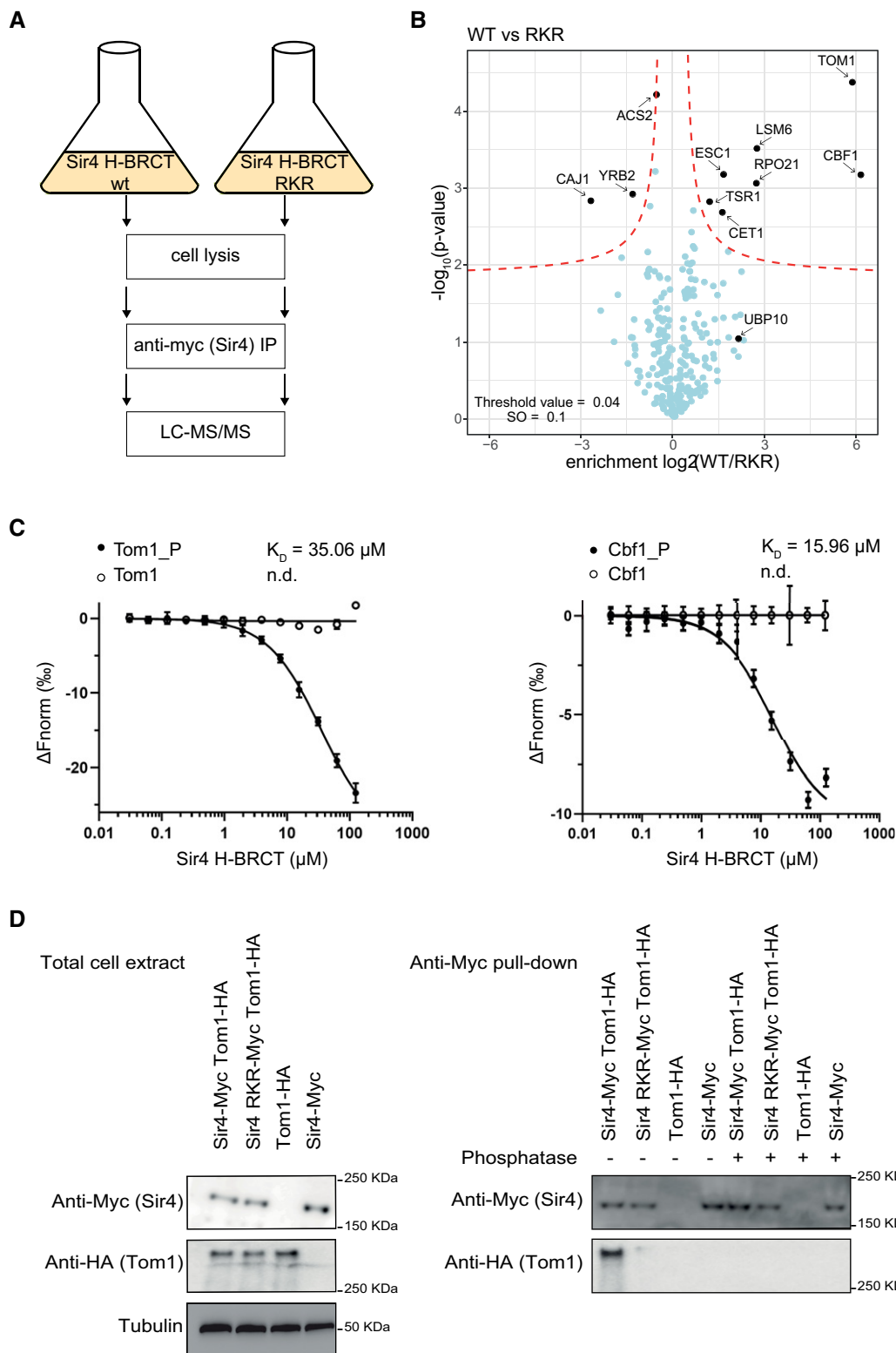


Figure 5.

**Figure 5. Sir4 H-BRCT interacts with Tom1 and Cbf1 in a phospho-dependent manner.**

- A Scheme of experimental design for IP-MS. Cells lacking endogenous *sir4* and expressing the Myc-tagged H-BRCT domain of Sir4, either wt or carrying mutations (RKR) were subjected to anti-Myc immunoprecipitation followed by LC-MS/MS analyses.
- B Volcano plot showing proteins that interact with wt Sir4 H-BRCT but not with the RKR mutant (upper right quadrant).
- C MST analysis of the binding interactions between Sir4 H-BRCT and Cy5-labeled phospho (filled circles) and non-phospho-peptides (empty circles) from Tom1 and Cbf1.  $K_D$  represents the equilibrium dissociation constant. The  $K_D$  for interactions with the non-phospho-peptides could not be determined (n.d.).  $\Delta F_{\text{norm}} [\%]$  represents the change in fluorescence during thermophoresis normalized to the initial fluorescence. Data are represented as the mean  $\pm$  SEM from at least three independent measurements.
- D Extracts from asynchronous cultures of strains Sir4-Myc Tom1-HA (GA-10645), Sir4-RKR-Myc Tom1-HA (GA-10646), Tom1-HA (GA-10647), and Sir4-Myc (GA-10199) were subjected to anti-Myc IP and Western blotting with indicated antibodies in the presence and absence of lambda phosphatase.

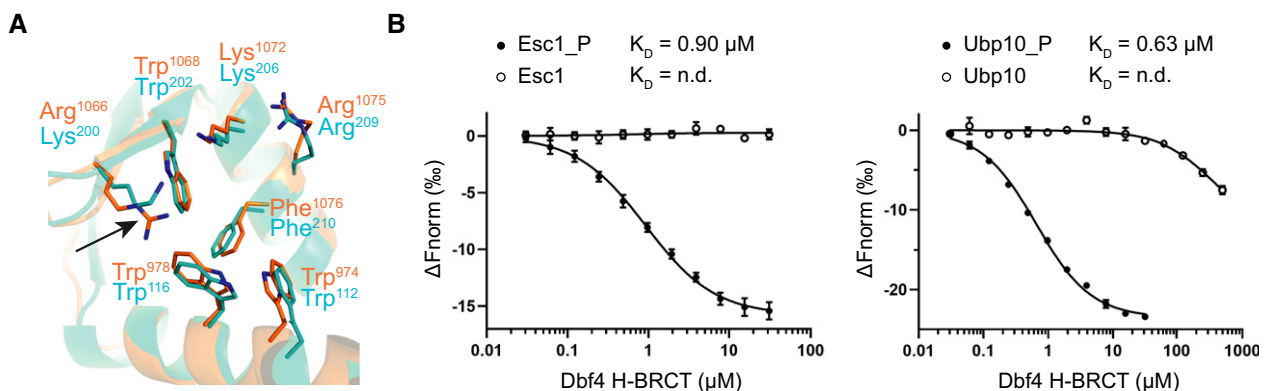
that this is due to the replacement of Arg1066 in Sir4 by Lys200 in Dbf4. This underscores both the conservation and the fine-tuning possible within this important class of non-canonical BRCT domains. We conclude that the H-BRCT domains of Dbf4 and Sir4 both bind phospho-peptides, although with differences in selectivity and affinity.

## Discussion

We describe a non-canonical H-BRCT domain in the budding yeast heterochromatin maintenance protein Sir4 and investigate in detail its capacity to interact with phosphorylated target proteins. BRCT domains are extensively studied phospho-peptide binder modules that were initially characterized in DNA damage response proteins, where they participate in a complex kinase signaling network that arrests the cell cycle in response to DNA damage and trigger DNA repair (Leung & Glover, 2011; Reinhardt & Yaffe, 2013). Classically, BRCT domains are associated in tandem in a tight head-to-tail fashion through a large hydrophobic interface over which they bind the pSxxF recognition motif of partner proteins through two main interactions. The phosphorylated serine is anchored through electrostatic interactions to the first BRCT domain, while the phenylalanine sits in a hydrophobic cleft of the second BRCT domain (Manke et al, 2003; Shiozaki et al, 2004).

More recent work has revealed a much broader versatility of this protein domain, going far beyond the phospho-peptide binding mode initially assigned to BRCA1's BRCT domain. For example, the tandem BRCTs of 53BP1 are a phosphorylation-independent protein-protein interaction module that forms a heterodimer with the DNA-binding domain of p53 (Derbyshire et al, 2002). The MRN complex component, Nbs1, has a tandem BRCT unit that coalesces with its FHA domain to bind a diphosphorylated pSer-Asp-pThr-Asp motif in Mdc1 (Lloyd et al, 2009), and multiple BRCT domains are present as single structural unit in TOPBP1 (Dbp11 in *S. cerevisiae*, Rad4 in *Schizosaccharomyces pombe*; Rappas et al, 2011). Intriguingly, individual BRCT domains in TOPBP1 bind a combinatorially diverse set of phospho-ligands of varying sequences that appear to adopt conformationally similar binding modes (Day et al, 2018). In other cases, single BRCT domains are used as adaptors to mediate binding in a phosphorylation-independent manner, as in the case of the XRCC1-DNA ligase III interaction or the budding yeast translesion synthesis DNA polymerase Rev1 interaction with PCNA (Dulic et al, 2001; Pustovalova et al, 2013). Finally, BRCT domains can also contact DNA, as in the case of human replication factor C p140 (Kobayashi et al, 2010), or the XRCC1 BRCT1 domain, which binds both poly(ADP-ribose) and DNA using two non-overlapping regions (Polo et al, 2019).

The H-BRCT variant found in Sir4 contains an N-terminal  $\alpha$ -helix attached to the BRCT core, that was first identified in the Dbf4

**Figure 6. Comparison between Sir4 and Dbf4 H-BRCT domains and phospho-peptide binding to Dbf4 H-BRCT.**

- A Superposition of Sir4 (orange) and Dbf4 (PDB 3QBZ, cyan) H-BRCT domains highlighting the structural conservation of the Sir4 phospho-epitope binding region in Dbf4. The only change is the Arg1066 (Sir4 H-BRCT) replacement to Lys200 (Dbf4 H-BRCT), highlighted by an arrow, while all other residues are conserved.
- B MST analysis of the binding interactions between Dbf4 H-BRCT and Cy5-labeled phospho (filled circles) and non-phospho-peptides (empty circles) from Esc1 and Ubp10.  $K_D$  = equilibrium dissociation constant, which could not be determined (n.d.) for non-phospho-peptides.  $\Delta F_{\text{norm}} [\%]$  represents the change in fluorescence during thermophoresis normalized to the initial fluorescence. Data are the mean  $\pm$  SEM from  $\geq 3$  independent measurements.

**Table 1. Binding motifs of phospho-peptides.**

	-2	-1		+1	+2	+3	$K_D$ (Sir4 H-BRCT) [ $\mu$ M]	$K_D$ (Dbf4 H-BRCT) [ $\mu$ M]
Esc1 <sup>pS1450</sup>	L	P	<b>pS</b>	D	P	P	0.07	0.90
Ubp10 <sup>pT123</sup>	L	S	<b>pT</b>	E	P	P	0.07	0.63
Ty5 <sup>pS1095</sup>	L	D	S	<b>pS</b>	P	P	5.57	n.d.
Tom1 <sup>pS2376</sup>	I	D	<b>pS</b>	D	F	L	35.06	75.46
Cbf1 <sup>pS155</sup>	M	T	<b>pS</b>	S	P	M	15.96	172.43

Consensus: [LIM]-x-[ST]-[SDE]-[PF]-[PLM].

Table listing interacting protein residues around the phospho-group (shown in bold) of phospho-peptides for which  $K_D$  values, from MST measurements, for Sir4 H-BRCT and Dbf4 H-BRCT binding were determined. A consensus motif is listed below the table.

regulatory subunit of the Dbf4-dependent kinase (DDK, Dbf4-Cdc7), where it is used to bind the FHA1 domain of Rad53 in a phosphorylation-independent manner (Matthews *et al*, 2012, 2014; Almawi *et al*, 2016). Here, we show that Dbf4 H-BRCT also has the capacity to bind to phosphorylated Esc1 and Ubp10 peptides, with nanomolar affinity, as does Sir4 H-BRCT. The Dbf4 H-BRCT-Ubp10 pT123 peptide binding may be physiologically relevant, given that Ubp10 stabilizes Dbf4 levels through deubiquitination in order to activate the Cdc7 kinase, allowing Cdc7-Dbf4 to phosphorylate the MCM helicase and catalyze the initiation of DNA replication at the G1/S transition (Mapa *et al*, 2018). This is further corroborated by the finding that deletion of the N-terminal intrinsically disordered region of Ubp10, which contains the Ubp10<sup>pT123</sup> peptide, leads to a reduction of Dbf4 levels and delays S-phase entry (Mapa *et al*, 2018). Further work is needed to determine whether the Dbf4 H-BRCT domain acts as versatile phospho-protein binder, as demonstrated for the Sir4 H-BRCT domain. Intriguingly, given that the putative phospho-epitope binding region in Dbf4 H-BRCT partially overlaps with the surface patch engaged in FHA1-Rad53 interaction (Almawi *et al*, 2016), the two binding modes may be mutually exclusive.

We have characterized biochemically and structurally the Sir4 H-BRCT domain and have shown that it is critical for Sir4's silencing function. Mutations in the Sir4 H-BRCT domain that disrupt phospho-epitope binding result in mislocalization of Sir4, most likely due to the loss of Sir4-Esc1 interaction, and loss of heterochromatic repression. The link to ubiquitin ligases through Sir4 may also contribute to heterochromatin formation and the nuclear localization of silent domains (Burgess *et al*, 2012; Gardner *et al*, 2005).

Our structural and biochemical data of Sir4 H-BRCT ligands suggest that an accessible phosphorylated sequence stretch containing the PROSITE string [LIM]-x-[ST]-[SDE]-[PF]-[PLM], where S/T are phosphorylated, characterizes interactors of the Sir4 H-BRCT (Table 1). Hydrophobic residues at positions -2 and +2, +3 with respect to the phosphorylation site, are required for interaction with indole rings of the double tryptophan motif and a double proline at +2, +3 positions results in tightest binding. Side chains of residues at position -1 point into solvent and contribute to binding only through their backbone atoms. Therefore, this position can probably be populated by any amino acid. The serine- or threonine-linked phospho-group interacts with the Arg1066, Trp1068, and Lys1072 triad while the +1 glutamate side chain in the case of Ubp10<sup>pT123</sup> is long enough to additionally engage Arg1075 in an electrostatic

interaction. Ty5<sup>pS1095</sup> also profits from Arg1075 and binds its guanidinium group at the +1 phosphorylated serine residue. Having the phospho-group shifted toward the C-terminus by one residue (+1 position) results in approximately tenfold lower affinity.

Based on measured affinity constants for peptides of varying sequences, structural insights, and the observation that a phospho-site at position +1 disfavors tight interaction, we defined an idealized consensus motif, [LI]-x-[ST]-[DE]-P-P, which is predicted to bind either Sir4 H-BRCT or Dbf4 H-BRCT. Using this consensus, we carried out a ScanProsite (<https://prosite.expasy.org/scanprosite/>) search against the yeast nuclear proteome (Gauci *et al*, 2009). The results (presented in Table EV5) show that the motif was found in just one protein, Mcm6, besides the well-characterized Sir4 interactors Esc1 and Ubp10. Mcm6 is a subunit of the heptameric minichromosome maintenance complex (MCM), and multiple MCM subunits are targets of the Dbf4-dependent kinase DDK (Larasati & Duncker, 2016), which is critical for the initiation of DNA replication. DDK docking sites have been mapped to MCM subunits 2/4, but our data suggest that the phospho-motif on Mcm6 (875-ITSEPP-880), located on a disordered stretch of the C-terminus, may contribute to DDK recruitment. Further investigations will be needed to validate this putative DDK docking site on the MCM complex.

A less stringent search string that allowed a phospho-site at position +1 and an additional hydrophobic residue of similar length at position -2, [LIM]-x-[STDE]-[STDE]-P-P, detected Ty5 and three additional proteins (Bir1, Taf10, and Tod6), which have not been characterized as Sir4 or Dbf4 interactors to date (Table EV5). Hits in the lower stringency search require biochemical and genetic analysis to establish whether or not these putative ligands have biological relevance.

Here, we report micromolar affinity of the Sir4 H-BRCT domain for a phosphorylated motif within the E3 ubiquitin ligase Tom1. Tom1 is required for cell cycle-dependent ubiquitination and degradation of Dia2, a component of the SCF<sup>Dia2</sup> E3 ubiquitin ligase involved in DNA replication (Kim & Koepf, 2012). Interestingly, Dia2 ubiquitylates Sir4 and cells lacking Dia2 show silencing defects in yeast heterochromatin (Burgess *et al*, 2012). Therefore, it is conceivable that Tom1 and Dia2 ubiquitin ligases are part of a cell cycle-dependent auto-regulatory loop that controls Sir4 levels. In short, we speculate that in the absence of phosphorylated Tom1, Dia2 is able to ubiquitylate Sir4, leading to its degradation. However, when Tom1 is phosphorylated and interacts with Sir4, it

may be able to ubiquitylate and degrade Dia2, thereby antagonizing the degradation of Sir4. It is well established that Sir4 dosage levels need to be tightly controlled in order to ensure gene silencing, as a single extra copy of *SIR4* disrupts silent chromatin (Cockell *et al*, 1995; Smith *et al*, 1998). It is possible that the controlled recruitment of Tom1 by Sir4 contributes to this homeostasis.

Heterochromatin assembly and disassembly is a dynamic cell cycle-dependent process regulated by phosphorylation and ubiquitylation events (Emre & Berger, 2006; Weake & Workman, 2008). An important conclusion from our study is that there is a non-canonical phospho-epitope binding H-BRCT domain in the heterochromatin scaffolding protein Sir4, which provides a platform for binding phosphorylated proteins. The phospho-epitope binding motif within Sir4 is shown to be essential for stable heterochromatin formation and for the sequestration of Sir4-tagged heterochromatic foci at the nuclear periphery.

## Materials and Methods

### Cloning, expression, and purification of H-BRCT and FHA1 domains

#### *Sir4* H-BRCT Se-Met and native versions

The region corresponding to aa 961–1,085 in UniProt entry P11978 from *S. cerevisiae* Sir4 was subcloned into pOPINF using InFusion cloning (Berrow *et al*, 2007) to yield an N-terminal His<sub>6</sub> tag with a 3C cleavage site between the tag and the protein of interest. Native Sir4 H-BRCT expression was performed in *E. coli* BL21 (DE3) Star cells through auto-induction for 20 h at 18°C. In the case of Se-Met derived Sir4 H-BRCT protein, expression was carried out in *E. coli* B834 (DE3) cells (Merck) induced by 0.5 mM IPTG in selenomethionine medium (Molecular Dimensions, UK) for 20 h at 20°C. Cell pellets were harvested and resuspended in nickel lysis buffer (50 mM Tris-Cl, pH 7.5, 150 mM NaCl, 1 mM TCEP, 2.5 mM MgCl<sub>2</sub>, 0.2% Tween-20), frozen on dry ice, and then stored at –80°C. The thawed cell suspension was diluted with cold nickel lysis buffer, freshly supplemented with Benzonase (Sigma) and Complete EDTA-free protease inhibitors (Roche), then filtered through Miracloth (Merck), and passed two times through the EmulsiFlex-C3 cell disruptor (Avestin Europe, GmbH) at 15,000 psi. The total cell lysate was centrifuged at 35,000 × *g* for 30 min at 4°C, and the soluble lysate was collected and filtered through a Minisart MNL Plus filter (Sartorius) prior to incubation in batch mode with Ni-NTA Superflow beads (Qiagen). The Ni-NTA beads were transferred into a Bio-Rad Econo column and washed with low-salt nickel wash buffer (50 mM Tris-Cl, pH 7.5, 150 mM NaCl, 1 mM TCEP), then with the same plus 500 mM NaCl, and again with 150 mM NaCl. Digestion with 1 mg His-tagged 3C protease was performed overnight at 4°C. Target protein was collected in the column flow-through and wash fractions, concentrated over an Amicon 10 kDa MWCO Ultra device to 4 ml, and separated on a gel-filtration S75 HiLoad column pre-equilibrated in GF buffer (20 mM Tris-Cl, pH 7.4, 200 mM NaCl, 2 mM TCEP). Peak fractions containing the target protein were pooled and concentrated to 1.91 mM (native wt), 4.57 mM (native RKR mutant), and 1.13 mM (Se-Met), and aliquots were snap-frozen in N<sub>2</sub>(liq) and stored at –80°C.

#### Dbf4 H-BRCT

The region corresponding to aa 99–250 in UniProt P32325 from *S. cerevisiae* Dbf4 was subcloned into pOPINF by InFusion cloning (Berrow *et al*, 2007), yielding an N-terminal His<sub>6</sub> tag with a 3C cleavage site followed by the H-BRCT domain (Matthews *et al*, 2012). A C-terminal extension of ~35 aa enhanced protein expression (Matthews *et al*, 2009). Dbf4 H-BRCT expression, purification, and storage were performed as described for the Sir4 H-BRCT domain, except that Tris buffers were at pH 8.0, and Dbf4 H-BRCT protein concentrates to 1.2 mM.

A construct encoding aa 29–158 of *S. cerevisiae* serine/threonine-protein kinase Rad53 (UniProt P22216), encompassing the FHA1 domain, was subcloned into pOPINF using InFusion cloning, generating an N-terminal His<sub>6</sub> tag and 3C cleavage site upstream of FHA1. Expression and purification were essentially as described for the H-BRCT domains. Following the Ni-NTA affinity column, an S75 HiLoad column was used, and purified His-tagged Rad53 was digested with 3C protease and passed over a Ni-NTA column, collected in the flow-through and first wash fractions. Purified Rad53 was concentrated over a 3 kDa MWCO Amicon filter, separated by gel filtration on a S75 HiLoad column, and concentrated in running buffer (20 mM Tris, pH 7.4, 200 mM NaCl, 1 mM TCEP, 0.02% NaN<sub>3</sub>) to 3.15 mg/ml (tagged) and 1.33 mg/ml (non-tagged), respectively.

#### Crystallization

Crystallization was carried out using the sitting-drop vapor diffusion method at 20°C with a Phoenix nano-liter dispensing robot (Art Robbins). Unbound Se-Met or native Sir4 H-BRCT crystals were obtained by mixing 200 nl protein at approximately 1 mM in 20 mM Tris, pH 7.5, 200 mM NaCl, 0.5 mM TCEP, 0.02% NaN<sub>3</sub>, with 100 nl Silver Bullet (condition F1, Hampton Research) and 100 nl crystallization buffer (35% PEG 2000 MME, 150 mM potassium bromide). Silver Bullet condition F1 consists of 0.25% (w/v) methylenediphosphonic acid, 0.25% (w/v) phytic acid sodium salt hydrate, 0.25% (w/v) sodium pyrophosphate tetrabasic decahydrate, 0.25% (w/v) sodium triphosphate pentabasic, 0.02 M HEPES sodium, pH 6.8. Plates were incubated at 4°C for 10 days; crystals were cryo-protected under crystallization conditions with 20 mM Tris, pH 7.5, and 15% ethylene glycol followed by cryo-cooling in N<sub>2</sub>(liq).

Sir4 H-BRCT-Esc1<sup>PS1450</sup> peptide co-crystals were obtained by mixing 100 μl of protein solution containing 1.0 mM Se-Met Sir4 H-BRCT and 1.36 mM Esc1<sup>PS1450</sup> phospho-peptide (aa 1,443–1,458: IPSTDLPPSDPPSDEKEE, Peptide Specialty Laboratories GmbH, Germany) in 0.02 M Tris pH 7.5, 0.2 M NaCl, 0.002 M TCEP, 0.02% NaN<sub>3</sub> with 100 μl of crystallization buffer containing 30% PEG4000, 0.2 M ammonium acetate, and 0.1 M Na-acetate pH 4.6. Rod-like crystals were cryo-protected in crystallization buffer with 20% ethylene glycol and 1.36 mM Esc1<sup>PS1450</sup> phospho-peptide followed by cryo-cooling in N<sub>2</sub>(liq).

Sir4 H-BRCT Ty5<sup>PS1095</sup> peptide co-crystals were obtained by mixing 100 μl of 1.0 mM Se-Met Sir4 H-BRCT and 2.7 mM Ty5<sup>PS1095</sup> phospho-peptide (aa 1,087–1,103: ESPPSLDspSPNTSFNA, Peptide Specialty Laboratories GmbH, Germany) in 0.02 M Tris pH 7.5, 0.2 M NaCl, 0.002 M TCEP, 0.02% NaN<sub>3</sub> with 100 μl of crystallization buffer containing 2.0 M (NH<sub>4</sub>)<sub>2</sub>SO<sub>4</sub>, 0.2 M Na-potassium tartrate, and 0.1 M Na<sub>3</sub>-citrate pH 5.6. Thin rod-like crystals were

cryo-protected in crystallization buffer with 3.2 M  $(\text{NH}_4)_2\text{SO}_4$  and 2.7 mM Ty5<sup>PS1095</sup> phospho-peptide followed by cryo-cooling in  $\text{N}_2(\text{liq})$ .

Sir4 H-BRCT-Ubp10<sup>PT123</sup> peptide co-crystals were obtained by mixing 100 nl of 1 mM native Sir4 H-BRCT protein with a 1.3 mM Ubp10<sup>PT123</sup> phospho-peptide (aa 117–128: LSTELSpTEPPSS, Peptide Specialty Laboratories GmbH, Germany) in 20 mM Tris, pH 7.5, 200 mM NaCl, 1 mM TCEP with 100 nl crystallization buffer containing 27.8% PEG 4000, 0.1 M Na-acetate, pH 4.9, 0.2 M ammonium acetate, and 3% w/v trimethylamine N-oxide hydrate. Rod-like crystals were cryo-protected under crystallization conditions with 1 mM Ubp10<sup>PT123</sup> phospho-peptide and 13% ethylene glycol followed by cryo-cooling in  $\text{N}_2(\text{liq})$ .

### Data collection, structure solution, and refinement

X-ray data collection was performed at SLS PX-II/III beamlines in Villigen, Switzerland, at 100 K. Diffraction images were processed and scaled using the XDS package (Kabsch, 2010). The structure of Sir4<sup>(961–1,085)</sup> was solved by the single anomalous diffraction method (SAD) using HKL2MAP (Pape & Schneider, 2004) with data collected at the peak wavelength ( $\lambda = 0.97903 \text{ \AA}$ ) of a selenomethionine derivative Sir4 H-BRCT crystal ( $C_2$  space group with one molecule in the asymmetric unit). Four selenium sites were located with SHELXD and used for phasing and density modification in SHELXE (Sheldrick, 2008), followed by automated model building in BUCCANEER (Cowtan, 2006). Models were manually completed in COOT (Emsley *et al.*, 2010) and refined in PHENIX (Adams *et al.*, 2010) and used for molecular replacement against a native data set later collected at 1.1 Å resolution. Further refinement used alternating cycles of manual rebuilding in COOT and refinement in PHENIX using anisotropic B-factor methods and explicit hydrogens.

Sir4 H-BRCT peptide co-crystal structures with Esc1<sup>PS1450</sup> (2.5 Å), Ty5<sup>PS1095</sup> (3.0 Å), and Ubp10<sup>PT123</sup> (2.18 Å) were solved by molecular replacement using the native Sir4 H-BRCT structure as search model with PHASER (McCoy *et al.*, 2007). The Sir4 H-BRCT-Esc1<sup>PS1450</sup> peptide complex crystallized in space group P1 with eight copies of the complex in the unit cell. Positive  $mF_o - DF_c$  difference electron density for the missing peptide allowed model building in all copies of Sir4 H-BRCT. The Sir4 H-BRCT-Ty5<sup>PS1095</sup> peptide complex crystallized in space group P4<sub>1</sub>2<sub>1</sub>2 with three copies of the complex in the asymmetric unit. Positive  $mF_o - DF_c$  difference electron density for the missing peptide was clearly visible and allowed model building in all Sir4 H-BRCT chains. The Sir4 H-BRCT-Ubp10<sup>PT123</sup> peptide crystals were space group P2<sub>1</sub> with seven peptide complexes in the asymmetric unit. Phospho-peptides were built into good quality, positive  $mF_o - DF_c$  difference electron density in all chains. Final structures for all peptide complexes were obtained by alternating rounds of manual rebuilding in COOT followed by structural refinement in PHENIX and Buster (Bricogne *et al.*, 2010). Final structures were validated using MolProbity (Chen *et al.*, 2010) and COOT. Structural images for figures were prepared with PyMOL (<http://pymol.sourceforge.net/>).

### Microscale thermophoresis

N-terminal Cy5-labeled peptides (Table EV3 for the sequences of peptides used) were synthesized by Peptide Specialty Laboratories

GmbH, Heidelberg, Germany. The peptides were prepared as 5 mM stocks in 0.1 M Tris, pH 8.0 and diluted to 100 nM in MST diluent (20 mM Tris, pH 7.5, 200 mM NaCl, 1 mM TCEP, 1% BSA, and 0.1% Tween-20). A twofold dilution series of Sir4 H-BRCT or Dbf4 H-BRCT protein was prepared in MST diluent and separately mixed 1:1 with Cy5-labeled peptide to give a fixed final concentration of 50 nM Cy5-labeled peptide. To study the effect of sulfate ions on H-BRCT binding to Ty5 peptides, 200 mM  $\text{Na}_2\text{SO}_4$  was used in place of the 200 mM NaCl in the MST diluent. The mixtures were incubated for 15 min in the dark and then loaded into premium capillaries and measured in a Monolith NT.115 (NanoTemper Technologies GmbH, Munich, Germany). The instrument settings were 25°C, 20% MST power, 20% LED power and nano-red with fluorescence before 5 s, MST on 30 s, fluorescence after 5- and 25-s delay. Measurements were performed using NT control software v2.1.31, and experiments were repeated independently  $\geq 3$  times. Data were analyzed using MO Affinity Analysis 2.3 (NanoTemper Technologies GmbH) using the signal from thermophoresis to calculate the binding affinities with the  $K_D$  fit model for a molecular interaction with a 1:1 stoichiometry.

### Thermofluor assay

SyproOrange (Sigma) was diluted 1,000-fold in 1.2 ml of sample buffer (20 mM Tris-HCl, pH 7.5, 300 mM NaCl, 1 mM TCEP). Twenty microliters of 10 mg/ml of wt or mutant RKR Sir4 H-BRCT was added to the diluted SyproOrange solution. Twenty-four different buffers were selected from the SlicePH screen (rows F-G from Hampton Research) and were diluted to 500 mM, and 10  $\mu\text{l}$  was dispensed in quadruplet into 96-well PCR plates (Thermo, AB-700). 10  $\mu\text{l}$  of the protein-SyproOrange solution was mixed with the 10  $\mu\text{l}$  buffer in the PCR plate, and the plate was sealed with iCycler optical tape (Bio-Rad) and centrifuged 500  $\times g$  for 1 min. Fluorescence was measured in a StepOne Plus (Applied Biosystems) real-time PCR machine. Data acquisition was done within the StepOne Plus software, running a melt curve experiment with ROX as the selected reporter, while the quencher and the passive reporter were set to zero. The temperature gradient started at 25°C, with increments of 1°C per minute, to 95°C. After each run, the experiments were analyzed and saved with the StepOne Plus software and then exported into Protein Thermal Shift software v1.3 (Applied Biosystems) to generate the mean of the quadruplet melting point derivatives. Each experiment was repeated three times for each domain. Figures were generated using GraphPad v8.1.

### SEC-MALS of H-BRCT domains

Quality and oligomeric status of purified H-BRCT domains were analyzed by size exclusion and multi-angle light scattering. Purified H-BRCT domains at 10 mg/ml or monomer BSA (Sigma) at 2 mg/ml were filtered through a 0.1- $\mu\text{m}$  Amicon filter before injecting 38  $\mu\text{l}$  onto a Superose 6 Increase 10/300 GL column (GE Healthcare) connected to an Agilent 1100 HPLC. Separation was carried out at 0.5 ml/min in 20 mM Tris, pH 7.5, 200 mM NaCl, and 1 mM TCEP. The UV, light-scattering miniDAWN TREOS, and refractive index Optilab T-rEx detectors (Wyatt Technology) were connected in series. Data analysis used the Zimm fitting method in Astra 6.1.1 software (Wyatt Technology), and figures were generated using GraphPad v8.1.

### SEC-MALS for Rad53 and Sir4 H-BRCT interaction

For Rad53 FHA1 and Sir4 H-BRCT interactions, untagged Rad53 FHA1 (1 mg/ml, 68  $\mu$ M) was incubated alone or with untagged Sir4 H-BRCT (4.4 mg/ml, 296  $\mu$ M) on ice for 3 h, and samples were filtered through an 0.1- $\mu$ m Amicon filter and 100  $\mu$ l was injected onto a Wyatt SEC 300  $\text{\AA}$  column coupled to an AKTA Basic FPLC connected in series to a light-scattering miniDAWN TREOS and refractive index Optilab T-rEx detectors (Wyatt Technology). Separations were at 4°C, in 20 mM Tris-Cl, pH 7.4, 200 mM NaCl, 1 mM TCEP, 0.02%  $\text{NaN}_3$  at flow rate 0.5 ml/min and were analyzed by the Zimm fitting method in Astra 6.1.1 software (Wyatt Technology). Figures were generated using GraphPad v8.1

### Yeast strains

All *S. cerevisiae* strains are described in Table EV4. Cells were grown using standard techniques (30°C in YPAD medium) for yeast strain generation and growth unless otherwise stated. For competition experiments, overexpression of Sir4 H-BRCT domain (either wt or carrying R1066A, K1072A, R1075A mutations) was achieved in yeast cells (Fig 4A: GA-10372, Fig 4D and E: GA-1981) by expressing Sir4 aa 961–1,085 in-frame with a nuclear localization signal at the N-terminus and a Myc-tag at the C-terminus from plasmid OGS3459 (Sigma).

### Silencing assays

Silencing of indicated reporter genes was performed as described (Gotta *et al*, 1998) after growth overnight in selective media. Five-fold dilution series starting at  $10^7$  cells/ml were performed in triplicates on appropriate media.

### Fluorescence microscopy

Cells were grown in synthetic complete (SC) media with 4 $\times$  additional adenine (72 mg/l) to prevent auto-fluorescence. Cells were fixed in fresh paraformaldehyde (PFA) 4% w/v for 5 min, washed six times in PBS, and then attached to a 0.17-mm glass coverslip using Concanavalin A. Images were captured on a Metamorph-driven Spinning-disk confocal system based on Olympus IX81 microscope equipped with a Yokogawa CSU-X1 scan head, EM-CCD cascade II (Photometrics) camera, and a ASI MS-2000 Z-piezo stage. We used a PlanApo  $\times$ 100, NA 1.45 total internal reflection fluorescence microscope oil objective and VisiView software. Fluorophores were excited at 561 nm (for RFP) and 491 nm (for GFP), and emitted fluorescence was acquired simultaneously on separate cameras. Image analysis was performed with NIH ImageJ.

### Immunoprecipitation and Western blotting

Immunoprecipitation was performed as in Deshpande *et al* (2017) with the following modifications: Myc-Trap (chromotek-ytma-20) magnetic beads were used to pull-down Sir4-Myc. Roche complete protease inhibitor tablets (Sigma-04693116001) were used at twice the recommended concentration to prevent Sir4/Tom1 degradation. Bead washing was performed in Lambda protein phosphatase buffer with or without 2,000 units of Lambda protein phosphatase

(NEB-P0753S). Samples were incubated for 30 min at 30°C and resuspended in Laemmli buffer. The following antibodies were used: anti-HA antibody (Santa Cruz sc-7392), anti-Tubulin antibody (Thermo Fisher Scientific MA1-8817), and anti-Myc antibody (in-house antibody service of the Friedrich Miescher Institute for Biomedical Research).

### Affinity purification for LC-MS/MS

Yeast cells (GA-1981) were transformed with the overexpression plasmid OGS3459 containing Sir4 H-BRCT either wt or with R1066A, K1072A, and R1075A. 50 ml of log-phase yeast cultures ( $\text{OD}_{600} = 0.5$ ) was harvested and washed once with ice-cold phosphate-buffered saline in the presence of Complete Protease Inhibitor Cocktail and PhosSTOP Phosphatase Inhibitor Cocktail (Roche). Cells were snap-frozen in  $\text{N}_2$ (liq). Thawed pellets were lysed in lysis buffer [50 mM HEPES pH 7.4, 150 mM NaCl, 2 mM EDTA, 0.5% NP-40, Complete Protease Inhibitor Cocktail, PhosSTOP Phosphatase Inhibitor Cocktail (Roche)], by bead-beating with Zirconia beads. Lysate was spun at 12,000 g, 10 min, 4°C, and the supernatant was filtered through a 0.45- $\mu$ m centrifugal filter. The cleared lysate was incubated with 8  $\mu$ l of Myc-Trap\_MA beads (ChromoTek) at 4°C for 4 h. Beads were washed with lysis buffer lacking NP-40 and protease inhibitor cocktail. The enriched proteins were digested directly on the Myc-Trap\_MA beads (ChromoTek) with 0.2  $\mu$ g Lys-C in 5  $\mu$ l digestion buffer (3 M guanidinium chloride, 20 mM EPPS pH 8.5, 10 mM CAA, 5 mM TCEP) for 2 h at RT. Next, samples were diluted with 50 mM HEPES pH 8.5 and digested with 0.2  $\mu$ g trypsin ON at 37°C, followed by 0.2  $\mu$ g fresh trypsin the next day, and incubating for 5 h more at 37°C.

### Mass spectrometry

The entire MS experiment was performed as biological triplicates. The generated peptides (see Affinity purification for LC-MS/MS) were acidified with TFA to a final concentration of 0.8% and loaded with 0.1% formic acid, 2% acetonitrile in  $\text{H}_2\text{O}$  onto a peptide trap (Acclaim PepMap 100, 75  $\mu\text{m} \times 2$  cm, C18, 3  $\mu\text{m}$ , 100  $\text{\AA}$ ) with an EASY-nLC 1000 (Thermo Scientific). Peptides were separated on a 50  $\mu\text{m} \times 15$  cm ES801 C18, 2  $\mu\text{m}$ , 100  $\text{\AA}$  column (Thermo Scientific) mounted on a DPV ion source (New Objective), at a flow rate of 150 nl/min with a linear gradient of 2–6% buffer B in buffer A in 3 min followed by an linear increase from 6 to 22% in 40 min, 22–28% in 9 min, 28–36% in 8 min, and 36–80% in 1 min, and the column was finally washed for 14 min at 80% B (buffer A: 0.1% formic acid, buffer B: 0.1% formic acid in acetonitrile). The data were acquired on a Orbitrap Fusion (Thermo Scientific) mass spectrometer using 120,000 resolution for the full scan in the Orbitrap and a top T (3 s) method with HCD fragmentation for each precursor and fragment measurement in the ion trap according the recommendation of the manufacturer (Thermo Scientific).

Protein identification and relative quantification of the proteins were done with MaxQuant version 1.5.3.8 using Andromeda as search engine (Cox *et al*, 2011) and label-free quantification (LFQ; Cox *et al*, 2014) as described in Hubner *et al* (2010). The *S. cerevisiae* UniProt version 2017\_04 combined with the contaminant DB from MaxQuant was searched with carbamidomethyl as a fixed modification on cysteine and variable modification oxidation on methionine, protein

N-terminus acetylation, and phosphorylation on serine, and threonine. The protein and peptide FDR were set to 0.01.

Statistical analysis was done in Perseus (version 1.5.8.5; Cox *et al*, 2011, 2014; Tyanova *et al*, 2016). Results were filtered to remove reverse hits, and contaminants and peptides found in only one sample. Missing values were imputed, and potential interactors were determined using *t*-test and visualized by a volcano plot (Fig 5B), showing only nuclear proteins as described by Gauci *et al* (2009). Significance lines corresponding to a given FDR have been determined by a permutation-based method (Tusher *et al*, 2001). Threshold values (FDR) were selected between 0.005 and 0.05 and  $S_0$  (curve bend) between 0.1 and 2 and are shown in the corresponding figures. Results were exported from Perseus and visualized using statistical computing language R.

## Data availability

The data sets produced in this study are available in the following databases:

- Atomic coordinates and structure factors: PDB 6RRV (Sir4 H-BRCT unbound; <https://www.rcsb.org/structure/6rrv>)
- Atomic coordinates and structure factors: PDB 6QSZ (Sir4 H-BRCT-Esc1<sup>pS1450</sup> complex; <https://www.rcsb.org/structure/6qsz>)
- Atomic coordinates and structure factors: PDB 6QTM (Sir4 H-BRCT-Ty5<sup>pS1095</sup> complex; <https://www.rcsb.org/structure/6qtm>)
- Atomic coordinates and structure factors: PDB 6RR0 (Sir4 H-BRCT-Ubp10<sup>pT123</sup> complex; <https://www.rcsb.org/structure/6rr0>)
- Protein interaction MS data: PRIDE PXD014119 (<http://www.ebi.ac.uk/pride/archive/projects/PXD014119>)

**Expanded View** for this article is available online.

## Acknowledgements

Part of this work was performed at beamlines X06DA and X10SA of the Swiss Light Source. The Friedrich Miescher Institute for Biomedical Research is supported by the Novartis Research Foundation and a grant from the Swiss National Science Foundation (31003A\_176286) to SMG.

## Author contributions

ID and HG conceived the study and designed experiments. JJK expressed, purified, and crystallized proteins. JJK and HG collected diffraction data and HG determined crystal structures. ID established yeast strains, did pull-downs for IP-MS, and performed yeast drop assays. KC did fluorescence microscopy, pull-down experiments, and drop assays. VI carried out mass spectrometry experiments and analysis. JJK performed and analyzed MST, SEC-MALS, and Thermofluor experiments. HG, ID, JJK, and SMG wrote the paper. HG and SMG supervised the work.

## Conflict of interest

The authors declare that they have no conflict of interest.

## References

Adams PD, Afonine PV, Bunkoczi G, Chen VB, Davis IW, Echols N, Headd JJ, Hung LW, Kapral GJ, Grosse-Kunstleve RW *et al* (2010) PHENIX: a

comprehensive Python-based system for macromolecular structure solution. *Acta Crystallogr D Biol Crystallogr* 66: 213–221

- Almawi AW, Matthews LA, Larasati, Myrox P, Boulton S, Lai C, Moraes T, Melacini G, Ghirlando R, Duncker BP, Guarne A (2016) 'AND' logic gates at work: crystal structure of Rad53 bound to Dbf4 and Cdc7. *Sci Rep* 6: 34237
- Andrulis ED, Zappulla DC, Ansari A, Perrod S, Laiosa CV, Gartenberg MR, Sternglanz R (2002) Esc1, a nuclear periphery protein required for Sir4-based plasmid anchoring and partitioning. *Mol Cell Biol* 22: 8292–8301
- Ansari A, Gartenberg MR (1997) The yeast silent information regulator Sir4p anchors and partitions plasmids. *Mol Cell Biol* 17: 7061–7068
- Aparicio OM, Billington BL, Gottschling DE (1991) Modifiers of position effect are shared between telomeric and silent mating-type loci in *S. cerevisiae*. *Cell* 66: 1279–1287
- Berrow NS, Alderton D, Sainsbury S, Nettleship J, Assenberg R, Rahman N, Stuart DI, Owens RJ (2007) A versatile ligation-independent cloning method suitable for high-throughput expression screening applications. *Nucleic Acids Res* 35: e45
- Brady TL, Fuerst PG, Dick RA, Schmidt C, Voytas DF (2008) Retrotransposon target site selection by imitation of a cellular protein. *Mol Cell Biol* 28: 1230–1239
- Brand AH, Micklem G, Nasmyth K (1987) A yeast silencer contains sequences that can promote autonomous plasmid replication and transcriptional activation. *Cell* 51: 709–719
- Bricogne G, Blanc E, Brandl M, Flensburg C, Keller P, Paciorek P, Roversi P, Sharff A, Smart O, Vonrhein C *et al* (2010) *BUSTER version 2.11.5*. Cambridge, UK: Global Phasing Ltd
- Buchman AR, Lue NF, Kornberg RD (1988) Connections between transcriptional activators, silencers, and telomeres as revealed by functional analysis of a yeast DNA-binding protein. *Mol Cell Biol* 8: 5086–5099
- Bupp JM, Martin AE, Stensrud ES, Jaspersen SL (2007) Telomere anchoring at the nuclear periphery requires the budding yeast Sad1-UNC-84 domain protein Mps3. *J Cell Biol* 179: 845–854
- Burgess RJ, Zhou H, Han J, Li Q, Zhang Z (2012) The SCFDia2 ubiquitin E3 ligase ubiquitylates Sir4 and functions in transcriptional silencing. *PLoS Genet* 8: e1002846
- Chang JF, Hall BE, Tanny JC, Moazed D, Filman D, Ellenberger T (2003) Structure of the coiled-coil dimerization motif of Sir4 and its interaction with Sir3. *Structure* 11: 637–649
- Chen VB, Arendall III WB, Headd JJ, Keedy DA, Immormino RM, Kapral GJ, Murray LW, Richardson JS, Richardson DC (2010) MolProbity: all-atom structure validation for macromolecular crystallography. *Acta Crystallogr D Biol Crystallogr* 66: 12–21
- Chen H, Xue J, Churikov D, Hass EP, Shi S, Lemon LD, Luciano P, Bertuch AA, Zappulla DC, Geli V *et al* (2018) Structural insights into yeast telomerase recruitment to telomeres. *Cell* 172: 331–343 e13
- Cockell M, Palladino F, Laroche T, Kyriou G, Liu C, Lustig AJ, Gasser SM (1995) The carboxy termini of Sir4 and Rap1 affect Sir3 localization: evidence for a multicomponent complex required for yeast telomeric silencing. *J Cell Biol* 129: 909–924
- Connelly JJ, Yuan P, Hsu HC, Li Z, Xu RM, Sternglanz R (2006) Structure and function of the *Saccharomyces cerevisiae* Sir3 BAH domain. *Mol Cell Biol* 26: 3256–3265
- Cowtan K (2006) The Buccaneer software for automated model building. 1. Tracing protein chains. *Acta Crystallogr D Biol Crystallogr* 62: 1002–1011
- Cox J, Neuhauser N, Michalski A, Scheltema RA, Olsen JV, Mann M (2011) Andromeda: a peptide search engine integrated into the MaxQuant environment. *J Proteome Res* 10: 1794–1805



- Cox J, Hein MY, Lubner CA, Paron I, Nagaraj N, Mann M (2014) Accurate proteome-wide label-free quantification by delayed normalization and maximal peptide ratio extraction, termed MaxLFQ. *Mol Cell Proteomics* 13: 2513–2526
- Cubizolles F, Martino F, Perrod S, Gasser SM (2006) A homotrimer-heterotrimer switch in Sir2 structure differentiates rDNA and telomeric silencing. *Mol Cell* 21: 825–836
- Dai J, Xie W, Brady TL, Gao J, Voytas DF (2007) Phosphorylation regulates integration of the yeast Ty5 retrotransposon into heterochromatin. *Mol Cell* 27: 289–299
- Day M, Rappas M, Ptasińska K, Boos D, Oliver AW, Pearl LH (2018) BRCT domains of the DNA damage checkpoint proteins TOPBP1/Rad4 display distinct specificities for phosphopeptide ligands. *Elife* 7: e39979
- Derbyshire DJ, Basu BP, Serpell LC, Joo WS, Date T, Iwabuchi K, Doherty AJ (2002) Crystal structure of human 53BP1 BRCT domains bound to p53 tumour suppressor. *EMBO J* 21: 3863–3872
- Deshpande I, Seeber A, Shimada K, Keusch JJ, Gut H, Gasser SM (2017) Structural basis of Mec1-Ddc2-RPA assembly and activation on single-stranded DNA at sites of damage. *Mol Cell* 68: 431–445.e5
- Dulic A, Bates PA, Zhang X, Martin SR, Freemont PS, Lindahl T, Barnes DE (2001) BRCT domain interactions in the heterodimeric DNA repair protein XRCC1-DNA ligase III. *Biochemistry* 40: 5906–5913
- Emre NC, Berger SL (2006) Histone post-translational modifications regulate transcription and silent chromatin in *Saccharomyces cerevisiae*. *Ernst Schering Res Found Workshop* 57: 127–153
- Emsley P, Lohkamp B, Scott WG, Cowtan K (2010) Features and development of Coot. *Acta Crystallogr D Biol Crystallogr* 66: 486–501
- Ferreira HC, Luke B, Schober H, Kalck V, Lingner J, Gasser SM (2011) The PIAS homologue Siz2 regulates perinuclear telomere position and telomerase activity in budding yeast. *Nat Cell Biol* 13: 867–874
- Gardner RG, Nelson ZW, Gottschling DE (2005) Ubp10/Dot4p regulates the persistence of ubiquitinated histone H2B: distinct roles in telomeric silencing and general chromatin. *Mol Cell Biol* 25: 6123–6139
- Gartenberg MR, Neumann FR, Laroche T, Blaszczyk M, Gasser SM (2004) Sir-mediated repression can occur independently of chromosomal and subnuclear contexts. *Cell* 119: 955–967
- Gartenberg MR, Smith JS (2016) The nuts and bolts of transcriptionally silent chromatin in *Saccharomyces cerevisiae*. *Genetics* 203: 1563–1599
- Gauci S, Veenhoff LM, Heck AJ, Krijgsveld J (2009) Orthogonal separation techniques for the characterization of the yeast nuclear proteome. *J Proteome Res* 8: 3451–3463
- Gotta M, Palladino F, Gasser SM (1998) Functional characterization of the N terminus of Sir3p. *Mol Cell Biol* 18: 6110–6120
- Hass EP, Zappulla DC (2015) The Ku subunit of telomerase binds Sir4 to recruit telomerase to lengthen telomeres in *S. cerevisiae*. *Elife* 4: e07750
- Hecht A, Laroche T, Strahl-Bolsinger S, Gasser SM, Grunstein M (1995) Histone H3 and H4 N-termini interact with SIR3 and SIR4 proteins: a molecular model for the formation of heterochromatin in yeast. *Cell* 80: 583–592
- Hecht A, Strahl-Bolsinger S, Grunstein M (1996) Spreading of transcriptional repressor SIR3 from telomeric heterochromatin. *Nature* 383: 92–96
- Hediger F, Neumann FR, Van Houwe G, Dubrana K, Gasser SM (2002) Live imaging of telomeres: yKu and Sir proteins define redundant telomere-anchoring pathways in yeast. *Curr Biol* 12: 2076–2089
- Holt LJ, Tuch BB, Villen J, Johnson AD, Gygi SP, Morgan DO (2009) Global analysis of Cdk1 substrate phosphorylation sites provides insights into evolution. *Science* 325: 1682–1686
- Hsu HC, Wang CL, Wang M, Yang N, Chen Z, Sternglanz R, Xu RM (2013) Structural basis for allosteric stimulation of Sir2 activity by Sir4 binding. *Genes Dev* 27: 64–73
- Hubner NC, Bird AW, Cox J, Spletstoesser B, Bandilla P, Poser I, Hyman A, Mann M (2010) Quantitative proteomics combined with BAC TransgeneOmics reveals *in vivo* protein interactions. *J Cell Biol* 189: 739–754
- Imai S, Armstrong CM, Kaerberlein M, Guarente L (2000) Transcriptional silencing and longevity protein Sir2 is an NAD-dependent histone deacetylase. *Nature* 403: 795–800
- Kabsch W (2010) Xds. *Acta Crystallogr D Biol Crystallogr* 66: 125–132
- Kim DH, Koepf DM (2012) Hect E3 ubiquitin ligase Tom1 controls Dia2 degradation during the cell cycle. *Mol Biol Cell* 23: 4203–4211
- Kobayashi M, Ab E, Bonvin AM, Siegal G (2010) Structure of the DNA-bound BRCA1 C-terminal region from human replication factor C p140 and model of the protein-DNA complex. *J Biol Chem* 285: 10087–10097
- Kozłowski LP, Bujnicki JM (2012) MetaDisorder: a meta-server for the prediction of intrinsic disorder in proteins. *BMC Bioinformatics* 13: 111
- Kueng S, Tsai-Pflugfelder M, Oppikofer M, Ferreira HC, Roberts E, Tsai C, Roloff TC, Sack R, Gasser SM (2012) Regulating repression: roles for the sir4 N-terminus in linker DNA protection and stabilization of epigenetic states. *PLoS Genet* 8: e1002727
- Kueng S, Oppikofer M, Gasser SM (2013) SIR proteins and the assembly of silent chromatin in budding yeast. *Annu Rev Genet* 47: 275–306
- Larasati, Duncker BP (2016) Mechanisms governing DDK regulation of the initiation of DNA replication. *Genes (Basel)* 8: E3
- Laroche T, Martin SG, Gotta M, Gorham HC, Pryde FE, Louis EJ, Gasser SM (1998) Mutation of yeast Ku genes disrupts the subnuclear organization of telomeres. *Curr Biol* 8: 653–656
- Leung CC, Glover JN (2011) BRCT domains: easy as one, two, three. *Cell Cycle* 10: 2461–2470
- Lloyd J, Chapman JR, Clapperton JA, Haire LF, Hartsuiker E, Li J, Carr AM, Jackson SP, Smerdon SJ (2009) A supramodular FHA/BRCT-repeat architecture mediates Nbs1 adaptor function in response to DNA damage. *Cell* 139: 100–111
- Luo K, Vega-Palas MA, Grunstein M (2002) Rap1-Sir4 binding independent of other Sir, yKu, or histone interactions initiates the assembly of telomeric heterochromatin in yeast. *Genes Dev* 16: 1528–1539
- Manke IA, Lowery DM, Nguyen A, Yaffe MB (2003) BRCT repeats as phosphopeptide-binding modules involved in protein targeting. *Science* 302: 636–639
- Mapa CE, Arsenault HE, Conti MM, Poti KE, Benanti JA (2018) A balance of deubiquitinating enzymes controls cell cycle entry. *Mol Biol Cell* 29: 2821–2834
- Marshall M, Mahoney D, Rose A, Hicks JB, Broach JR (1987) Functional domains of SIR4, a gene required for position effect regulation in *Saccharomyces cerevisiae*. *Mol Cell Biol* 7: 4441–4452
- Matthews LA, Duong A, Prasad AA, Duncker BP, Guarne A (2009) Crystallization and preliminary X-ray diffraction analysis of motif N from *Saccharomyces cerevisiae* Dbf4. *Acta Crystallogr Sect F Struct Biol Cryst Commun* 65: 890–894
- Matthews LA, Jones DR, Prasad AA, Duncker BP, Guarne A (2012) *Saccharomyces cerevisiae* Dbf4 has unique fold necessary for interaction with Rad53 kinase. *J Biol Chem* 287: 2378–2387
- Matthews LA, Selvaratnam R, Jones DR, Akimoto M, McConkey BJ, Melacini G, Duncker BP, Guarne A (2014) A novel non-canonical forkhead-associated (FHA) domain-binding interface mediates the interaction between Rad53 and Dbf4 proteins. *J Biol Chem* 289: 2589–2599

- McCoy AJ, Grosse-Kunstleve RW, Adams PD, Winn MD, Storoni LC, Read RJ (2007) Phaser crystallographic software. *J Appl Crystallogr* 40: 658–674
- Moazed D, Kistler A, Axelrod A, Rine J, Johnson AD (1997) Silent information regulator protein complexes in *Saccharomyces cerevisiae*: a SIR2/SIR4 complex and evidence for a regulatory domain in SIR4 that inhibits its interaction with SIR3. *Proc Natl Acad Sci USA* 94: 2186–2191
- Moretti P, Freeman K, Coodly L, Shore D (1994) Evidence that a complex of SIR proteins interacts with the silencer and telomere-binding protein RAP1. *Genes Dev* 8: 2257–2269
- Murphy GA, Spedale EJ, Powell ST, Pillus L, Schultz SC, Chen L (2003) The Sir4 C-terminal coiled coil is required for telomeric and mating type silencing in *Saccharomyces cerevisiae*. *J Mol Biol* 334: 769–780
- Onishi M, Liou GG, Buchberger JR, Walz T, Moazed D (2007) Role of the conserved Sir3-BAH domain in nucleosome binding and silent chromatin assembly. *Mol Cell* 28: 1015–1028
- Oppikofer M, Kueng S, Martino F, Soeroes S, Hancock SM, Chin JW, Fischle W, Gasser SM (2011) A dual role of H4K16 acetylation in the establishment of yeast silent chromatin. *EMBO J* 30: 2610–2621
- Oppikofer M, Kueng S, Gasser SM (2013) SIR-nucleosome interactions: structure-function relationships in yeast silent chromatin. *Gene* 527: 10–25
- Pape T, Schneider TR (2004) HKL2MAP: a graphical user interface for macromolecular phasing with SHELX programs. *J Appl Crystallogr* 37: 843–844
- Polo LM, Xu Y, Hornyak P, Garces F, Zeng Z, Hailstone R, Matthews SJ, Caldecott KW, Oliver AW, Pearl LH (2019) Efficient single-strand break repair requires binding to both Poly(ADP-Ribose) and DNA by the central BRCT domain of XRCC1. *Cell Rep* 26: 573–581 e5
- Pustovalova Y, Maciejewski MW, Korzhnev DM (2013) NMR mapping of PCNA interaction with translesion synthesis DNA polymerase Rev1 mediated by Rev1-BRCT domain. *J Mol Biol* 425: 3091–3105
- Rappas B, Oliver AW, Pearl LH (2011) Structure and function of the Rad9-binding region of the DNA-damage checkpoint adaptor TopBP1. *Nucleic Acids Res* 39: 313–324
- Reed BJ, Locke MN, Gardner RG (2015) A conserved deubiquitinating enzyme uses intrinsically disordered regions to scaffold multiple protein interaction sites. *J Biol Chem* 290: 20601–20612
- Reinhardt HC, Yaffe MB (2013) Phospho-Ser/Thr-binding domains: navigating the cell cycle and DNA damage response. *Nat Rev Mol Cell Biol* 14: 563–580
- Renauld H, Aparicio OM, Zierath PD, Billington BL, Chhablani SK, Gottschling DE (1993) Silent domains are assembled continuously from the telomere and are defined by promoter distance and strength, and by SIR3 dosage. *Genes Dev* 7: 1133–1145
- Rine J, Herskowitz I (1987) Four genes responsible for a position effect on expression from HML and HMR in *Saccharomyces cerevisiae*. *Genetics* 116: 9–22
- Roy R, Meier B, McAinsh AD, Feldmann HM, Jackson SP (2004) Separation-of-function mutants of yeast Ku80 reveal a Yku80p-Sir4p interaction involved in telomeric silencing. *J Biol Chem* 279: 86–94
- Rudner AD, Hall BE, Ellenberger T, Moazed D (2005) A nonhistone protein-protein interaction required for assembly of the SIR complex and silent chromatin. *Mol Cell Biol* 25: 4514–4528
- Rusche LN, Kirchmaier AL, Rine J (2002) Ordered nucleation and spreading of silenced chromatin in *Saccharomyces cerevisiae*. *Mol Biol Cell* 13: 2207–2222
- Schober H, Ferreira H, Kalck V, Gehlen LR, Gasser SM (2009) Yeast telomerase and the SUN domain protein Mps3 anchor telomeres and repress subtelomeric recombination. *Genes Dev* 23: 928–938
- Sheldrick GM (2008) A short history of SHELX. *Acta Crystallogr A* 64: 112–122
- Shiozaki EN, Gu L, Yan N, Shi Y (2004) Structure of the BRCT repeats of BRCA1 bound to a BACH1 phosphopeptide: implications for signaling. *Mol Cell* 14: 405–412
- Shore D, Stillman DJ, Brand AH, Nasmyth KA (1987) Identification of silencer binding proteins from yeast: possible roles in SIR control and DNA replication. *EMBO J* 6: 461–467
- Sievers F, Wilm A, Dineen D, Gibson TJ, Karplus K, Li WZ, Lopez R, McWilliam H, Remmert M, Soding J et al (2011) Fast, scalable generation of high-quality protein multiple sequence alignments using Clustal Omega. *Mol Syst Biol* 7: 539
- Smith JS, Brachmann CB, Pillus L, Boeke JD (1998) Distribution of a limited Sir2 protein pool regulates the strength of yeast rDNA silencing and is modulated by Sir4p. *Genetics* 149: 1205–1219
- Soding J, Biegert A, Lupas AN (2005) The HHpred interactive server for protein homology detection and structure prediction. *Nucleic Acids Res* 33: W244–W248
- Strahl-Bolsinger S, Hecht A, Luo K, Grunstein M (1997) SIR2 and SIR4 interactions differ in core and extended telomeric heterochromatin in yeast. *Genes Dev* 11: 83–93
- Sussel L, Shore D (1991) Separation of transcriptional activation and silencing functions of the RAP1-encoded repressor/activator protein 1: isolation of viable mutants affecting both silencing and telomere length. *Proc Natl Acad Sci USA* 88: 7749–7753
- Swygert SG, Senapati S, Bolukbasi MF, Wolfe SA, Lindsay S, Peterson CL (2018) SIR proteins create compact heterochromatin fibers. *Proc Natl Acad Sci USA* 115: 12447–12452
- Taddei A, Hediger F, Neumann FR, Bauer C, Gasser SM (2004) Separation of silencing from perinuclear anchoring functions in yeast Ku80, Sir4 and Esc1 proteins. *EMBO J* 23: 1301–1312
- Tanner KG, Landry J, Sternglanz R, Denu JM (2000) Silent information regulator 2 family of NAD-dependent histone/protein deacetylases generates a unique product, 1-O-acetyl-ADP-ribose. *Proc Natl Acad Sci USA* 97: 14178–14182
- Tsukamoto Y, Kato J, Ikeda H (1997) Silencing factors participate in DNA repair and recombination in *Saccharomyces cerevisiae*. *Nature* 388: 900–903
- Tusher VG, Tibshirani R, Chu G (2001) Significance analysis of microarrays applied to the ionizing radiation response. *Proc Natl Acad Sci USA* 98: 5116–5121
- Tyanova S, Temu T, Sinitcyn P, Carlson A, Hein MY, Geiger T, Mann M, Cox J (2016) The Perseus computational platform for comprehensive analysis of (prote)omics data. *Nat Methods* 13: 731–740
- Weake VM, Workman JL (2008) Histone ubiquitination: triggering gene activity. *Mol Cell* 29: 653–663
- Zou S, Ke N, Kim JM, Voytas DF (1996) The *Saccharomyces* retrotransposon Ty5 integrates preferentially into regions of silent chromatin at the telomeres and mating loci. *Genes Dev* 10: 634–645
- Zukowski A, Al-Afaleq NO, Duncan ED, Yao T, Johnson AM (2018) Recruitment and allosteric stimulation of a histone-deubiquitinating enzyme during heterochromatin assembly. *J Biol Chem* 293: 2498–2509